Full title:

Sex-Specific Ethylene Responses and Convergent Plasticity: Multi-Omic Insights into *Cannabis* Sexual Plasticity

Short title:

Multi-Omic Insights into *Cannabis* sexual plasticity

Adrian S. Monthony[1,2,3,4], Julien Roy[1,2,3,4], Maxime de Ronne[1,2,3,4], Olivia Carlson[5], Susan J. Murch[5] & Davoud Torkamaneh[1,2,3,4*]

[1]Département de phytologie, Université Laval, Québec City, Québec, Canada

[2]Institut de Biologie Intégrative et des Systèmes (IBIS), Université Laval, Québec, Canada

[3]Centre de recherche et d'innovation sur les végétaux (CRIV), Université Laval, Québec, Canada

[4]Institut intelligence et données (IID), Université Laval, Québec, Canada

[5]Department of Chemistry, University of British Columbia, Kelowna, Canada

Monthony ORCID: 0000-0003-0536-691X

Roy ORCID: 0009-0002-9768-9096

de Ronne ORCID: 0000-0003-4062-3512

Murch ORCID: 0000-0001-5803-9483

*Torkamaneh ORCID: 0000-0002-9782-5695

*Corresponding Author

Email: davoud.torkamaneh.1@ulaval.ca

Abstract

Cannabis sativa exhibits remarkable sexual plasticity, with both XX and XY plants capable of phenotypic sex reversal in response to ethylene modulation. However, the molecular mechanisms underlying this process remain poorly characterized. Here, we applied a multi-omic framework—integrating transcriptomics, metabolite quantification, and whole-genome sequencing—to study the regulatory basis of ethylene-mediated sexual plasticity across three genetically distinct cannabis genotypes. We show that sex reversal induced by silver thiosulfate (XX masculinization) and ethephon (XY feminization) results in >80% floral sex conversion across genotypes. Despite a shared phenotypic response, transcriptomic analysis of 47 ethylene-related genes (ERGs) revealed a temporally dynamic and sex-specific response: a shared early-phase upregulation of biosynthesis and signaling genes at Day 1, followed by divergent gene expression patterns at Day 14 associated with phenotypic stabilization. Network analysis identified 14 candidate ERGs, including *CsMTN*, *CsACS1*, *CsACO3*, *CsACO5* and *CsERF1*, as key regulators of plasticity. Genomic variant profiling and chromosomal localization further revealed low nucleotide diversity in most ERGs, with several key genes localized exclusively to X chromosome's non-recombinant regions and notably, absent from the Y non-recombinant region. Together, our findings demonstrate that ethylene-mediated sex change in *C. sativa* involves temporally distinct transcriptional programs that differ between XX and XY plants and affirm that sexual plasticity does not exclusively rely on sex chromosome-linked genes. This study provides a high-resolution molecular framework for dissecting and ultimately controlling sexual plasticity in *C. sativa*, identifies candidate targets for functional validation, and lays the groundwork for breeding sex-stable genotypes in cannabis and other dioecious crops.

Keywords: cannabis, sex determination, transcriptomics, multi-omics, sexual plasticity, ethylene, silver thiosulfate, ethephon

Introduction

Cannabis sativa L. (cannabis) is diploid species (2n=20) with nine autosomes and one pair of XX/XY sex chromosomes (Lapierre *et al.*, 2023a; Monthony *et al.*, 2024). Cannabis produces indeterminate compound inflorescences that develop distinctly dimorphic flowers: female flowers (FFs) consist of an ovary, surrounded by two bracts, dotted with glandular trichomes and two pistils (Reed, 1914; Spitzer-Rimon *et al.*, 2019), while male flowers (MFs) are staminate, characterized by a segmented perianth and five hanging stamen (Reed, 1914). The glandular trichomes found on FFs synthesize medicinally important cannabinoids, of which over 100 have been characterized and are of interest for their potential medicinal applications (Giese *et al.*, 2015; Mudge *et al.*, 2019). In contrast, MFs produce cannabinoids at significantly lower levels and are considered to have negligible value in medicinal or commercial cannabis applications (Welling *et al.*, 2021). Most drug-type cannabis is dioecious, producing exclusively male (XY) or female (XX) flowers, though some monoecious plants, mostly industrial hemp, produce both on the same plant (Ferfuia *et al.*, 2021). Unlike most species—where the presence or absence of the Y chromosome alone determines sex—cannabis exhibits remarkable sexual plasticity—a plant's ability to alter its phenotypic sex in response to environmental or hormonal cues (Monthony *et al.*, 2024). Under normal growth conditions the phenotypic sex of cannabis plants is concordant with sex chromosome karyotype. However, documented cases of hermaphroditism and monoecy have been reported to arise spontaneous and from human intervention (Kurtz *et al.*, 2020; Punja & Holmes,

2020). Although the cannabis genome has been sequenced and assembled (Grassa *et al.*, 2021), and interest in sex determination is growing (Prentout *et al.*, 2020; Adal *et al.*, 2021; Shi *et al.*, 2024b), the molecular pathways underlying sex expression remain poorly understood. Thus, understanding the genetic and hormonal regulation of flower development and sex determination in cannabis has significant implications for both basic plant biology and applied cultivation strategies.

Sexual plasticity, which has also been referred to as leaky sex expression and sexual lability (Käfer *et al.*, 2022), has been described across diverse taxa of flowering monoecious and dioecious plants, including: *Carica papaya* (papaya; dioecious), *Spinacia oleracea* (spinach; dioecious), *Mercurialis annua* L. (monoecious) and *Amborella trichopoda* (dioecious) (Komai & Masuda, 2004; Sather *et al.*, 2010; Lin *et al.*, 2016; Anger *et al.*, 2017; Cossard & Pannell, 2021). However, the triggers of shifts in phenotypic sex or floral sex ratios differ widely among species and conditions, and include natural population variability (Anger *et al.*, 2017), reproductive pressure (Ji *et al.*, 2016; Cossard & Pannell, 2021), abiotic or biotic stressors (Lin *et al.*, 2016), and targeted molecular and plant growth regulator interventions (Thomas, 2004; Zhang *et al.*, 2017; García *et al.*, 2020). Although the precise molecular mechanisms controlling sexual plasticity in cannabis remain poorly understood, anecdotal reports from underground cultivators and subsequent empirical validation by academic researchers strongly indicates that ethylene signaling modulates sex expression in this species (Green, 2005; Lubell & Brand, 2018; Moon *et al.*, 2020; Jones & Monthony, 2022). Known ethylene signaling inhibitors, such as silver thiosulfate (STS), reliably induce male flowers (IMFs) in XX cannabis plants, while treatment with the ethylene-releasing compound ethephon (commercially Ethrel®) consistently promotes female flower development

(IFFs) in XY plants (Lubell & Brand, 2018; Moon *et al.*, 2020; Flajšman *et al.*, 2021). Similar regulatory roles of ethylene have been extensively studied in the Cucurbitaceae family, where increases in endogenous ethylene or exogenous applications result in an increased ratio of female to male flowers, resulting in ethylene often being described as feminizing (Rajagopalan *et al.*, 2004; Li *et al.*, 2021). Research on Cucurbitaceae has resulted in a well-characterized genetic network involving key ethylene biosynthesis and signaling genes, such as the ACC SYNTHASE (ACS), ACC OXIDASE (ACO), and ETHYLENE RESPONSE (ETR) family of genes (Boualem *et al.*, 2015; Zhang *et al.*, 2017; Li *et al.*, 2021), but beyond cucurbits, the role of ethylene as a central regulator of sexual plasticity has not been widely established, making the *C. sativa* a potentially interesting dioecious analogue to Cucurbitaceae. Recently, our research group presented a first integrative model of the ethylene precursor pathway, the Yang cycle (extensively review by Chen *et al.*, 2025), as well as ethylene biosynthesis and signaling pathways in cannabis (Monthony et al., 2024). This study generated an initial set of candidate ethylene-related genes (ERGs) hypothesized to govern sexual plasticity, supported by preliminary transcriptomic evidence and leveraging existing genetic datasets (Prentout *et al.*, 2020; Adal *et al.*, 2021). This model, as well as most studies of cannabis sex to date, have focused on the role of ERGs in IMF production, neglecting to consider whether XY feminization relies on reciprocal molecular and hormonal mechanisms.

Sexual plasticity is a complex, multi-layered process that likely involves coordination across genetic, transcriptomic, hormonal, and metabolic networks. Yet, to date, no dedicated multi-omic study has studied ERGs or characterized the molecular and hormonal dynamics underlying ethylene-mediated sexual plasticity across both XX and XY *Cannabis sativa* plants. Previous

transcriptomic snapshots paired with gene ontology (GO) analyses, produced extensive lists of differentially expressed genes with limited biological context (Prentout *et al.*, 2020; Adal *et al.*, 2021; Orozco *et al.*, 2025). While valuable in early exploratory phases, such approaches are inherently limited in their ability to distinguish genes directly involved in a specific biological process from those broadly responsive to development or stress—an issue well-documented in transcriptomic and GO-based studies across plant systems (Uygun *et al.*, 2016). These limitations are further compounded by biases introduced through incomplete GO annotations, inconsistent term specificity, and limited taxon relevance—challenges that are especially pronounced in non-model species like cannabis (Gaudet & Dessimoz, 2017; Fattel & Lawrence-Dill, 2025).

Cannabis sex determination and sexual plasticity research has continued to prioritize broad transcriptomic surveys—focused solely on sexual plasticity in XX plants—without addressing the reciprocal process in XY plants. More importantly, these studies are rarely centered around understanding the role of plant growth regulators (PGRs) such as ethylene, despite decades of phenotypic and experimental evidence implicating it as a central regulator of sex expression (Ram & Jaiswal, 1972; Galoch, 1978; Kurtz *et al.*, 2020; Moon *et al.*, 2020; Flajšman *et al.*, 2021; Monthony *et al.*, 2024). As the field matures, it is important to begin moving beyond descriptive surveys and toward integrative, hypothesis-driven study of sexual plasticity. A multi-omic framework—combining transcriptomic, metabolomic, and genomic data—enables higher-resolution interrogation of temporally dynamic regulatory networks and facilitates the identification of biologically grounded molecular mechanisms. In this study, we apply such an approach to elucidate the ethylene-responsive gene networks that govern cannabis sexual plasticity.

The high heterozygosity and phenotypic diversity of *C. sativa* present major challenges for generalizing biological findings from single-genotypes studies (Monthony *et al.*, 2021c; Page *et al.*, 2021). To address this, it is important to investigate ethylene-mediated sexual plasticity across multiple genetically distinct genotypes with divergent cannabinoid profiles, allowing for a broader understanding of species-level responses. Another limitation of existing studies is the narrow focus on floral tissues during sex transition. This approach implicitly assumes that sex-determining signals arise only once flowers are visibly developing. However, in many plants species, key floral fate regulators—such as FLOWERING LOCUS T (FT)—are activated in leaves in response to photoperiod changes and then transported to the shoot apical meristem to trigger flowering (Tsuji, 2017). Recently, evidence has emerged to support *C. sativa* following this conserved model, suggesting that *C. sativa* FT-like genes are responsive to photoperiod changes prior to the emergences of flowers (Dowling *et al.*, 2024).

By analyzing both genotypic and pre-floral tissue variation, our study offers a more complete view of the ethylene-responsive signaling networks coordinating sexual plasticity in cannabis. Our findings reveal that this process is not governed by a single genetic switch but is instead a temporally dynamic process involving distinct sets of genes. We identify genes likely involved in the initiation of sex change shortly after treatment, as well as others that contribute to stabilizing the new phenotypic state. Together, these results support a dynamic, phase-dependent model of ethylene-regulated sexual plasticity in cannabis.

Materials & Methods

Plant selection and vegetative growing conditions

Vegetative mother and father plants from three commercially available drug-type genotypes—*La Rosca*, *Panama Pupil V4*, and *Deadly Kernel*—were greenhouse-grown, cloned, and rooted for two weeks under LED lighting (Phlizon, China) in moistened stone wool (Indoor Farmer, Canada) beneath vented plastic humidity domes. Rooted clones were then transferred to 10 cm square pots filled with sterilized Pro-Mix BX (Pro-Mix, Canada) and maintained under controlled environment conditions in growth chambers (Conviron, Canada) for 10 days to allow root establishment. During this period, plants were watered by hand as needed.

Subsequently, plants were transplanted into 4-litre round pots and grown for 12 days under a 12/12 day/night photoperiod with drip irrigation adjusted weekly. Thereafter, the photoperiod was shifted to 18/12 to induce flowering. Photon flux density (PPFD), as well as day and night humidity levels, were gradually decreased throughout the experiment, reaching a maximum of 750 μmol/m²/s at canopy height, as detailed in Supplementary Table 1. The pH of the growth substrate was monitored weekly and maintained between 5.5 and 6.0, adjusted as necessary using 1.5 g/L of elemental sulfur during watering. A complete description of growing conditions, including photoperiod, light intensity, and fertigation regimes, is provided in Supplementary Table 1.

Plant sexing

Samples were taken the 6-month-old vegetative mother and father for all three drug-type genotypes to confirm the chromosomal sex. Approximately 50 mg of young leaf tissue was harvested for DNA extraction and desiccated for four days using Drierite (Xenia, OH, USA). The dried tissue was ground using metallic beads in a RETSCH MM 400 mixer mill (Fisher Scientific, MA, USA) and DNA was extracted using a CTAB-chloroform protocol (Lapierre *et al.*, 2023b). Briefly, powdered tissue was treated with CTAB buffer, followed by phenol-chloroform extraction. The resulting DNA pellet was washed with ethanol, resuspended in water, and quantified using a Qubit fluorometer with the dsDNA HS assay kit (Thermo Fisher Scientific, Waltham, MA, USA). DNA concentrations were adjusted to 10 ng/µL.

Sex determination was performed using PCR Allelic Competitive Extension (PACE, 3CR Bioscience Ltd) assay using CSP-2 primers (**Supplementary Table 2**) and methodology as described in Toth (2022), and Toth *et al.* (2020). PACE reactions were performed with PACE 2.0 Genotyping Master Mix (3CR Bioscience Ltd) and thermally cycled according to the manufacturer's instructions, with five extra final cycles (i.e. a total of 35 cycles of denaturation, annealing and extension) on the Applied Biosystems Veriti Thermal Cycler. Post-PCR fluorescence signals were detected with the Applied Biosystems 7500 Real-Time PCR System and analyzed using Applied Biosystems 7500 Software v2.3.

Plant flowering and sex plasticity induction

All plants were cultivated under LED lighting in controlled-environment growth chambers. To prevent pollination and accommodate space constraints, plants were grown in two separate batches under identical conditions (Supplementary Table 1). The first batch contained male flowering treatments: MF (XY) and IMF (XX), while the second batch contained female flowering treatments: FF (XX) and IFF (XY). Induction of sexual plasticity in XX plants was performed using STS, following the protocol of Jones & Monthony (2022). A 3 mM silver thiosulfate (STS) solution with 0.1% Tween 20 was prepared from sodium thiosulfate (Fisher Chemical, Fair Lawn, NJ, USA) and silver nitrate (Fisher Chemical, USA). The solution was applied as a foliar spray (~50 mL per plant) once per week for three weeks, ensuring thorough leaf coverage. The first application coincided with the photoperiod shift, immediately after the first 12-hour night, and all subsequent treatments were administered immediately after growth chamber lights extinguished in order to prevent leaf burning.

Induction of sexual plasticity in XY plants was achieved using 500 mg/L ethephon, adapted from Moon et al. (2020). The treatment solution was prepared from a 40% aqueous solution of ethephon (2-chloroethylphosphonic acid; AK Scientific, Union City, CA, USA), by diluting it in distilled water to the final concentration (500 mg/L; 8.65 mM) with 0.1% Tween 20 as a surfactant. Plants were sprayed to saturation (~50 mL per plant) in a single application, administered immediately after the photoperiod shift when growth chamber lights extinguished, to prevent leaf burning. In both batches, control plants (MF and FF) were sprayed to saturation with distilled water containing 0.1% Tween 20 to ensure comparable treatment conditions.

Floral development and quantification of sexual plasticity

Floral development was tracked weekly for 28 days following floral induction. Representative floral clusters were selected from the top half of the plant for macroscopy. Plants were visualized using an Olympus SZX16 macroscope (Olympus Corp., Japan) and photographed with an Olympus DP21 camera. Sexual plasticity was quantified by determining the ratio of flowers on six randomly selected inflorescence segments measuring 3 cm whose phenotypic sex no longer matched the plants genotypic sex. This was done following 28 days of flowering. For control plants (MF and FF), which displayed no sexual plasticity, one randomly selected inflorescence segment was selected.

Floral sex ratios were calculated in R (v4.1.1). A two-way fixed effects analysis of variance (ANOVA) was conducted. Sex change (%) was the response variable, genotype and phenotypic floral sex were the independent variables. Prior to analysis of variance, the sex change data were transformed using an arcsine square root transformation (McDonald, 2014), as the datasets for sex change (in percentiles) were highly clustered at 0 and 1, and the arcsine square root model shows less dramatic variance at the end of the distribution (Monthony *et al.*, 2021a). Means comparisons was performed using a Tukey-Kramer post-hoc test (Kramer, 1956) to account for multiple comparisons. Post-hoc means comparisons were visualized using the *multcompLetters4* from the multcompView package (Piepho, 2004). Bar plots of the average sex change were generated with ggplot2 (v3.4.1; Wickham, 2009) using the Paired colour palette from RColorBrewer (Brewer *et al.*, 2002).

Cannabinoid quantification

Cannabinoid quantification was performed using an established UPLC-PDA method, as previously described by Lapierre et al. (2023b), at the Metabolomics Platform, Institute of Nutrition and Functional Foods (INAF), Université Laval, Québec, QC, Canada. In brief, plants were grown under standard greenhouse conditions to maturity, as outlined in Lapierre et al. (2023b) and mature female (XX) flowers (~5 g) were collected, trimmed and dried for analysis. A subsample (200 mg) was extracted in 25 mL of 80% methanol (Thermo Fisher Scientific, Optima™ HPLC ≥99%) by sonication for 15 min. Extracts were centrifuged at 4500 × g for 5 min, and the supernatant was filtered through a 0.22 µm nylon filter before being diluted by factors of 2 and 20.

Cannabinoid analysis was performed using a Waters Acquity I-Class UPLC system with a photodiode array (PDA) UV detector. Separation was achieved on a Cortecs 1.6 µm, 2.1 mm × 150 mm column (Waters Corporation, Milford, MA, USA) with a Cortecs C18 pre-column (Waters Corporation, 90Å, 1.6 µm, 2.1 mm X 5 mm) maintained at 30°C. The mobile phase consisted of (A) 20 mM ammonium formate (Thermo Fisher Scientific, Optima LC/MS ≥99%), acidified to pH 2.92 with formic acid (MS grade) and diluted with Mili-Q water (Thermo Fisher Scientific) and (B) 100% acetonitrile (Milipore Sigma, OmniSolv® LC/MS ≥99.9%), with a gradient elution program as follows: 0–6.4 min, 76% B; 6.5–8 min, 99% B; 8.1–10 min, re-equilibration at 76% B. The flow rate was set at 0.45 mL/min, and the injection volume was 1 µL.

Detection was performed at 228 nm, and quantification was based on 5-point calibration curves (1–100 mg/L) for all cannabinoid standards.

Standard calibration curves were prepared by diluting a mix of cannabinoid standards in 80% methanol. A 500 µL stock solution at 100 mg/L was prepared by combining 50 µL of each individual standard from stock solutions at 1000 mg/L and adjusting the final volume with 80% methanol. Serial dilutions were then performed to generate calibration points at 100, 50, 25, 5, and 1 mg/L. Details of the cannabinoid standards are provided in Supplementary Table **3**.

Quantification of ACC and SAM

A detailed methodological description of standards preparation, derivatization, and chromatographic conditions is provided in the Supplementary Materials and the accompanying parameters can be found in Supplementary Table 4 through Supplementary Table 9. SAM and ACC concentrations were quantified against standard calibration curves prepared from serial dilutions of frozen stock standards, and lysine was included as an internal derivatization control (Supplementary Table 4 and Supplementary Table 5). Leaf tissues (n = 3 biological replicates per genotype, treatment, and time point) were harvested on day 0 and day 1, flash frozen, and extracted using a trichloroacetic acid (TCA) protocol (Bishop et al., 2024; Sandhu et al., 2024). Approximately 50 mg of leaf tissue was homogenized in 1 mL TCA, centrifuged, and filtered. Supernatants were derivatized using 6-aminoquinolyl-N-hydroxysuccinimidyl carbamate (AQC) (Supplementary Table 5) and analyzed via UPLC-MS/MS on a Waters Acquity I-Class UPLC and Xevo TQ-S system (Supplementary Table 6 & Supplementary Table 7). Chromatographic

separation was performed on a BEH C18 column, and analytes were detected in positive ESI mode using multiple reaction monitoring (MRM; Supplementary Table 8). SAM and ACC data processing for quantification was performed using TargetLynx V4.1 (Supplementary Table 9).

Statistical analysis of ACC and SAM data

VST-transformed gene expression data were correlated with measured ACC levels using Spearman's rank correlation within each treatment group. Genes with zero variance were excluded, and outliers (Studentized residuals > ±3.4) were removed. FDR correction was applied to p-values, and only genes with $|\rho| \geq 0.5$ and FDR-adjusted $p \leq 0.05$ in at least one group were visualized. ACC concentrations were also analyzed using a linear mixed-effects model including treatment, sex, and day as fixed effects, and sample ID nested within genotype as a random effect. Tukey's HSD post-hoc test was applied to estimated marginal means. SAM was below the limit of quantification in all samples and was not included in downstream analyses. Full statistical methods, R package versions, and model diagnostics are available in the Supplementary Materials.

ERG Identification

Identification of ERG in *C. sativa* was previously conducted using an *in silico* ortholog analysis by Monthony *et al.* (2024), based on the *C. sativa* cs10 reference genome (RefSeq assembly accession: GCF_900626175.2; Grassa *et al.*, 2021). We improve upon this dataset by applying the same methodology to newly available genomic resources, including the *C. sativa* 'Pink Pepper' XX reference genome (NCBI, 2023) and the haploid X and Y whole genomes for the genotype 'Otto II' (Carey *et al.*, 2024b). Briefly, ERG orthologs were identified using OrthoFinder (Emms

& Kelly, 2015) and BLASTP (Altschul *et al.*, 1990), as described in Monthony et al. (2024), followed by manual curation. Chromosome maps were generated with the chromoMap (v4.1.1; Anand & Rodriguez Lopez, 2022) package in R.

Whole genome sequencing and variant calling

Fresh leaf tissues obtained from one male (XY) and one female (XY) individual of the three genotypes were used for DNA extraction using the Qiagen DNeasy Plant Mini kit (Qiagen GmbH, Germany). For whole genome sequencing (WGS), six libraries were prepared at the Institut de biologie intégrative et des systèmes (IBIS), Université Laval, QC, Canada. The sequencing was conducted on an Illumina NovaSeq 6000 (Illumina, CA, USA) with 150 bp paired-end reads at the Genome Quebec Service and Expertise Center (CESGQ), Montreal, QC, Canada, with an average coverage of approximately 30x per sample.

Reads were mapped on the *C. sativa* 'Pink Pepper' reference genome (NCBI, 2023) with *bwa mem* version 7.17 (Li, 2013). Variant calling was performed with Fast-WGS (Torkamaneh *et al.*, 2018) and manta version 1.6 (Chen *et al.*, 2016a) for nucleotide and structural variant calling, respectively. Raw variant data were filtered with VCFtools version 1.16 (Danecek *et al.*, 2011) to remove low-quality variants (filter PASS, QUAL <10, MQ <30, MinDP <6, MAF 1%). Variants within ±5 kb of CsERGs in the *C. sativa* 'Pink Pepper' reference genome (NCBI, 2023) were filtered using BEDtools v2.31.1 (Quinlan & Hall, 2010). Functional impact of variants in ±5 kb around of CsERGs were investigated using the Ensembl Variant Effect Predictor (McLaren *et al.*, 2016) with the GFF of Pink Pepper (NCBI, 2023). Consequence terms (e.g., inframe insertion,

missense variant, synonymous variant) and the impact rating are based on Sequence Ontology (Eilbeck *et al.*, 2005). Impact ratings are classified as (i) Modifier correspond to variant affecting non-coding sequences, (ii) Low correspond to variant unlikely to change protein behaviour, (iii) Moderate correspond non-disruptive variant that might change protein effectiveness, and (iv) High correspond to variants probably causing protein truncation and/or loss of function. The nucleotide diversity (π; Nei & Li, 1979) in a sliding windows of 1000 bp and Tajima's D value in bins with size of 10,000 SNPs were estimated using VCFtools (Danecek *et al.*, 2011). Gene with less than 2 SNPs were excluded from the diversity analysis.

RNA extraction & sequencing

Leaf tissues were consistently sampled from mature leaves, in the middle section of the plant. Representative floral tissues (day 14) were consistently sampled from upper most axillary branch of the plants. Immediately after harvesting, plant tissues were flash-frozen in liquid nitrogen and hand-ground using a disposable cryosafe pestle in 2 mL RNase-free tubes to preserve RNA integrity. Total RNA was extracted using the RNeasy Plant Mini Kit (Qiagen), following the manufacturer's protocol with modifications to enhance RNA purity. Briefly, 25–50 mg of ground, frozen tissue was combined with RLC buffer and β-mercaptoethanol, as per the manufacturer's recommendations, and vortexed until homogenized. To improve purity, an additional wash with buffer RPE (Qiagen) was included in the final wash step. RNA was quantified spectrophotometrically using a NanoDrop spectrophotometer (Thermo Fisher Scientific). RNA quality was assessed visually, via electropherograms from the 2100 Bioanalyzer (Agilent Technologies, Santa Clara, CA, USA), and quantitatively, using the RNA Integrity Number (RIN; Supplementary Table 10). High-quality RNA samples were converted to cDNA using the

NEBNext® Ultra™ II Directional RNA Library Prep Kit for Illumina (New England Biolabs, Ipswich, MA, USA). Library preparation and sequencing were conducted at the Institut de Biologie Intégrative et des Systèmes (IBIS), Université Laval, Quebec, Canada. Sequencing was performed on an Element Biosciences AVITI platform (Element Biosciences, San Diego, CA, USA), generating 150 bp paired-end reads, with an average output of ~30 million reads per sample. In total, 138 samples passed quality control and were used in all future analyses (Supplementary Table 10).

Transcriptomic analysis

RNA sequencing quality was assessed using FASTQC (v0.11.8), and trimming of low-quality bases was performed in paired-end mode using Trimmomatic (v0.39) with the following parameters: adapter trimming (ILLUMINACLIP), a mismatch seed value of 2, a palindrome clip threshold of 30, a simple clip threshold of 10, and a minimum read length (MINLEN) of 40. For rare RNA samples identified with foreign RNA contamination based on overrepresented sequences and skewed GC ratios, contaminant sequences were extracted for further analysis. These sequences were classified by species using a BLAST search against the NCBI nucleotide database, with duplicates filtered and mapped to unique organisms. Non-plant contaminants, such as animal and fungal sequences, were removed using a modified Trimmomatic script with a custom contaminant sequence list. The trimming process retained ~95% of paired reads, and post-trimming quality was re-assessed using FastQC to confirm improvements in sequence composition.

Alignment of paired-end reads was performed as described in Monthony et al. (2024). Briefly, the paired-end reads were aligned to the *C. sativa* 'Pink Pepper' reference genome (NCBI) using STAR (v2.7.11b) with the output sorted by coordinate in BAM format (--outSAMtype BAM SortedByCoordinate). Gene-level counts were generated directly during alignment using STAR's --quantMode GeneCounts option. Post-alignment, the BAM files were filtered using Samtools to retain only reads with a mapping quality score (MAPQ) of 30 or higher (samtools view -b -q 30), ensuring high-confidence alignments, and quality was verified using Qualimap (v.2.2.1; Okonechnikov *et al.*, 2015), the results of which can be found in Supplementary Table 10. These filtered BAM files were then used to quantify gene expression levels using HTSeq-count (v2.0.2), as previously described in Monthony et al. (2024), with the following modifications: The MAPQ count filter was set to 30 (-a 30) to include both uniquely and multi-mapped reads, aligning with the MAPQ filter applied during STAR alignment. Reads were sorted by position, strandedness was considered, and gene counts were based on exons (-t exon) and identified using gene IDs (-i gene_id).

Principal component analysis and gene expression visualization

Principal component analysis (PCA) was performed on the VST normalized, batch-corrected counts of 47 selected genes of interest, obtained from gene-level counts following alignment and quantification. VST transformation was applied using the DESeq2 package (v1.42.1; Love *et al.*, 2014) to normalize the gene expression data. The first two principal components (PC1 and PC2) were extracted and plotted to visualize the clustering of samples based on their gene expression profiles. PCA plots were generated using the ggplot2 package (v3.5.1), with ellipses representing 95% confidence intervals for each treatment group.

For heatmap preparation, the filtered gene expression data was scaled by row (z-score transformation) using the pheatmap package (v1.0.12) to normalize gene expression levels across samples. Hierarchical clustering of genes and samples was performed using Euclidean distance and complete linkage to reveal patterns in gene expression across different treatments and time points.

Network analysis (WGCNA)

Weighted Gene Co-expression Network Analysis (WGCNA) was performed to construct sex-specific gene co-expression networks, identifying gene expression patterns associated with sex-change treatments. All analyses were performed in R (v4.3.3) using the WGCNA package (v1.73; Langfelder & Horvath, 2008). Networks were built separately for male (XY) and female (XX) samples, using count data processed through multiple quality control and normalization steps to ensure data integrity.

Prior to network construction, outlier genes and samples were detected and removed using the goodSamplesGenes (gsg) function in WGCNA, which identifies genes and samples with excessive missing values or abnormal expression patterns (see Supplementary Table 10). To further validate sample quality, hierarchical clustering and principal component analysis (PCA) were used to identify additional outlier samples, which were subsequently removed. Following outlier removal, batch correction was performed using a DESeq2-based method (Roy *et al.*, 2025). Additionally, low-count genes were filtered using HTSFilter (v1.42.0; Rau *et al.*, 2013), which dynamically

adjusts filtering thresholds based on dataset structure rather than applying an arbitrary cutoff. After filtering, the data were normalized using variance stabilizing transformation (VST) to reduce heteroscedasticity and improve network construction.

To determine an appropriate soft-thresholding power, the pickSoftThreshold function was applied independently to each subset to ensure scale-free topology (signed $R^2 > 0.80$ with minimal mean connectivity). Based on topology evaluation, a soft-thresholding power of 6 was selected for XX and 7 for XY datasets. Networks were constructed using blockwiseModules, employing a signed adjacency matrix, a module merging cut height of 0.20, with a maximum block size of 30,000 and modules were identified using dynamic tree cutting.

Module-trait correlation, adapted from Wang *et al.* (2020), was performed independently for XX and XY networks to identify biologically relevant gene clusters associated with sex-altering treatment. Treatment was defined as STS application in the XX network and ethephon application in the XY network. To prioritize biologically relevant gene modules, modules significantly correlated with treatment ($|r| \geq 0.5$, $p \leq 0.05$) were retained for further analysis (Wang *et al.*, 2020). To assess whether treatment-associated modules exhibited temporal specificity, their correlation with time points was examined. Time points were analyzed using a "Day vs. all" approach, where Day 1 and Day 14 were each compared to all other time points. Day was treated as a categorical variable with Day 0 as the baseline, while treatment was encoded as a binary variable (1 = treated, 0 = control). A shortlist of ethylene-related genes (ERGs) was generated by extracting those present in highly correlated modules. For each ERG, intra-modular connectivity (kME) was

calculated to assess its centrality within its respective module. The final list of ERGs from highly correlated modules in both XX and XY networks was retained for subsequent differential gene expression analysis.

Differential gene expression analysis

Differential gene expression (DGE) analysis was performed using DESeq2 to identify genes exhibiting significant expression changes in response to ethephon and STS treatments across male (XY) and female (XX) plants, respectively. DGE was focused on candidate ERGs identified in WGCNA. Raw count data were preprocessed by filtering low-expression genes using HTSFilter (Rau *et al.*, 2013). Normalized counts were obtained using variance stabilizing transformation (VST). Batch effects were modeled as a fixed effect in the DESeq2 generalized linear model (GLM) to correct for potential variation across experimental batches. Pairwise contrasts were constructed to evaluate: (1) STS-treated IMF (XX) vs. untreated FF (XX), (2) ethephon-treated IFF (XY) vs. untreated MF (XY), and (3) baseline differences between control MF (XY) and FF (XX) samples. Custom contrast vectors were applied to account for sex, treatment, and batch effects, ensuring robust comparisons. The $\log_2$ fold-change ($\log_2$FC) for each contrast was shrunk using ashr (Stephens, 2017) to provide more stable effect size estimates, particularly for low-expression genes.

Genes were considered significantly differentially expressed if they met the criteria of adjusted p-value (padj) ≤ 0.05 and absolute $\log_2\text{FC} \geq 1$ (Shi *et al.*, 2024b; Monthony *et al.*, 2024). Differentially expressed genes were further filtered to only include those differentially expressed

across all three genotypes, ensuring treatment effects were not genotype dependent. Visualization of DGE results included bar plots of $\log_2$FC values, highlighting genes with significant changes across treatment conditions and time points. Additionally, variance-stabilized expression levels were plotted using boxplots to compare expression profiles across MF, FF, IMF, and IFF groups. All analyses were conducted using R (v4.3.3), and visualizations were produced using ggplot2 (v3.5.1) for data visualization, dplyr (v1.1.4) for data manipulation, and wesanderson (v0.3.7) for color palettes.

Results

Highly inducible sexual plasticity in XX and XY cannabis

The ability of cannabis to exhibit sexual plasticity was evaluated by quantifying the percentage of flowers in the inflorescence whose phenotypic sex is opposite to the plant's chromosomal sex. A two-way fixed effects analysis of variance (ANOVA) was performed to assess the effects of treatment and genotype on the percentage of sex change, 28 days following the switch to a flowering photoperiod (12/12). Treatment had a significant effect on the extent of sex change ($p < 0.001$), whereas genotype ($p = 0.07$) and the interaction between genotype and treatment ($p = 0.91$) were not significant (Supplementary Table 11). Across all three genotypes, treated inflorescences exhibited average sex change rate > 80% (Table 1). In contrast, H_2O treated control plants showed no evidence of sexual plasticity in any genotype (Table 1). The observed phenotypic changes in treated plants are visually presented in Figure 1 and Supplemental Figure 1.

Table 1 Percentage of florets in *C. sativa* inflorescences that changed sex in response to sex plasticity induction treatments. FF- female flowers; MF- male flowers; IFF- induced female

flowers; IMF- induced male flowers. Uncertainty indicated by standard error of the mean (SEM) and differing letters indicate significant differences between treatments ($p \leq 0.05$), as determined by a Tukey-Kramer post-hoc test.

Sex	Treatment	Genotype	Sex Change (%)
XX	Control	Deadly Kernel	
		La Rosca	0.0 ± 0.0^{a}
		Panama Pupil V4	
XY	Control	Deadly Kernel	
		La Rosca	0.0 ± 0.0^{a}
		Panama Pupil V4	
XY	Treated (Ethephon)	Deadly Kernel	96.3 ± 2.6^{b}
		Panama Pupil V4	89.9 ± 4.0^{b}
		La Rosca	89.0 ± 5.6^{b}
XX	Treated (STS)	Deadly Kernel	94.7 ± 1.0^{b}
		La Rosca	92.5 ± 1.0^{b}
		Panama Pupil V4	80.5 ± 5.0^{b}

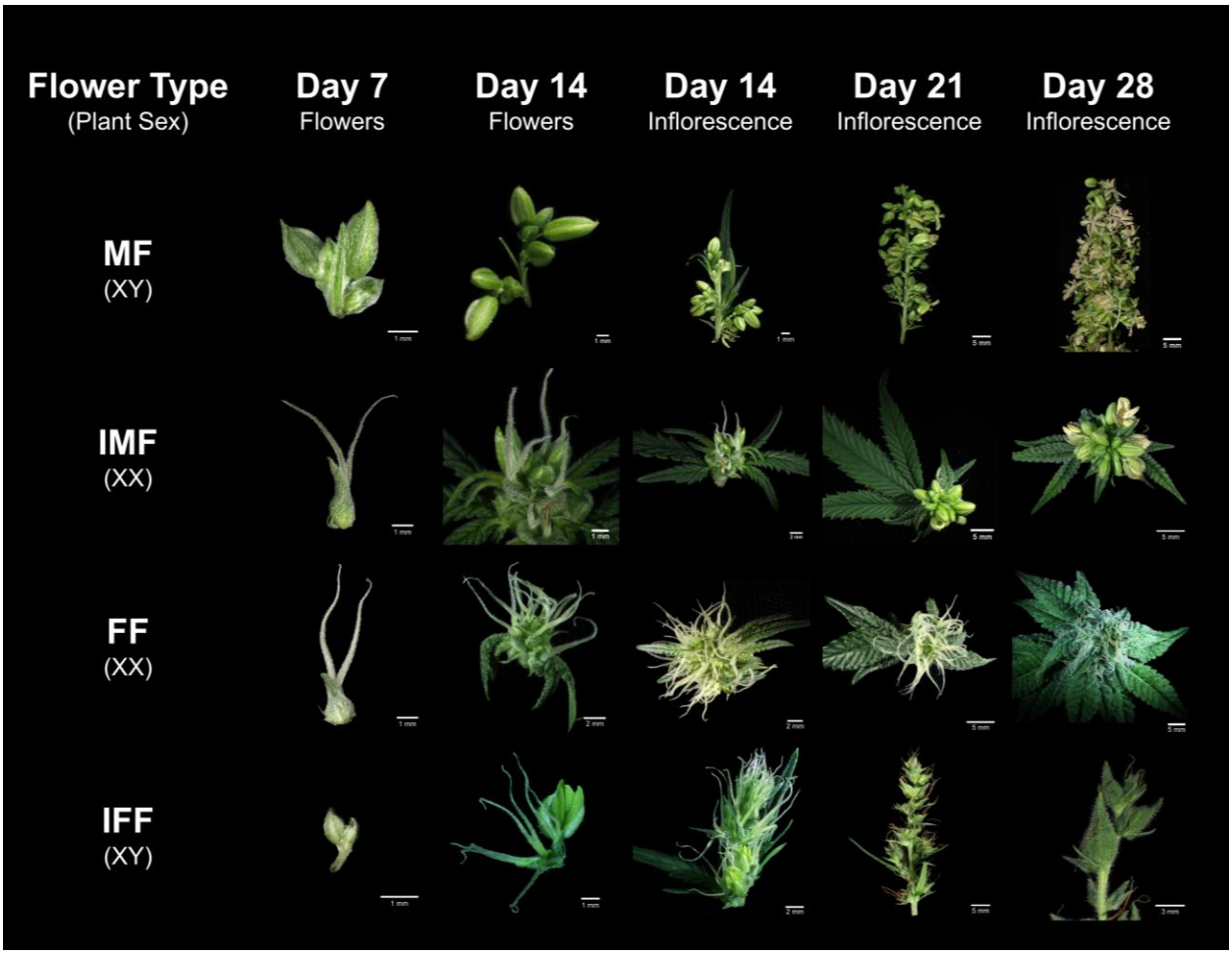

Figure 1 Representative timeline of floral development in MF, IMF, FF and IFF of *C. sativa* 'La Rosca' from 7 to 28 days after the photoperiod shift from long day to short day.

Cannabinoid analysis of control female flowers obtained from the three XX genotypes confirmed THC-dominance (Chemotype I; Zheng, 2022), with total THC content ranging from 16.98% to 25.40% w/w (Supplementary Table 12). Minor cannabinoids such as CBGA (0.28–1.20% w/w) and CBG (0.04–0.12% w/w) were also detected at varying levels (Supplementary Table 12).

An updated ortholog identification reveals X-specific ERGs

An updated ortholog analysis identified six additional putative ERGs, expanding upon previous findings (Monthony *et al.*, 2024). This analysis utilized newly available *C. sativa* genomes, including the new 'Pink Pepper' reference genome (NCBI, 2023) and a fully phased X and Y-haplotype genomes from a male Otto II genotype (Carey *et al.*, 2024b). In total, 47 ERGs were identified across the *C. sativa* genome (Supplementary Table 13), with the highest numbers found on chromosomes 1 and X (Figure 2A).

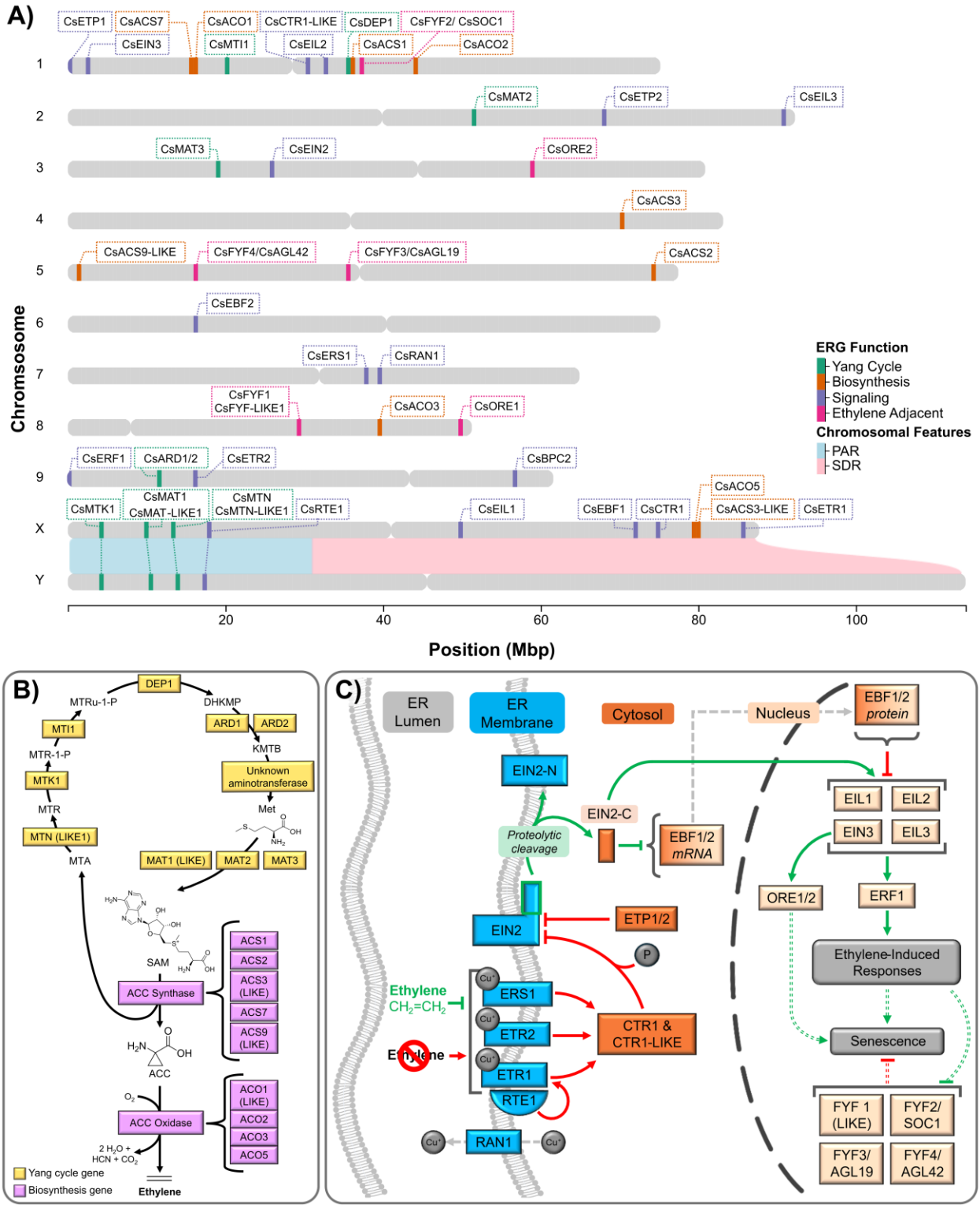
A)
CsETP1
CsACS7
CsACO1
CsCTR1-LIKE
CsDEP1
CsFYF2/ CsSOC1
CsEIN3
CsMTI1
CsEIL2
CsACS1
CsACO2
CsMAT2
CsETP2
CsEIL3
CsMAT3
CsEIN2
CsORE2
CsACS3
CsACS9-LIKE
CsFYF4/CsAGL42
CsFYF3/CsAGL19
CsACS2
CsEBF2
CsERS1
CsRAN1
CsFYF1
CsFYF-LIKE1
CsACO3
CsORE1
CsERF1
CsARD1/2
CsETR2
CsBPC2
CsACO5
CsMTK1
CsMAT1
CsMAT-LIKE1
CsMTN
CsMTN-LIKE1
CsRTE1
CsEIL1
CsEBF1
CsCTR1
CsACS3-LIKE
CsETR1
Chromosome
1
2
3
4
5
6
7
8
9
X
Y
20
40
60
80
100
Position (Mbp)
ERG Function
Yang Cycle
Biosynthesis
Signaling
Ethylene Adjacent
Chromosomal Features
PAR
SDR
B)
DEP1
MTRu-1-P
DHKMP
MTI1
ARD1
ARD2
MTR-1-P
KMTB
MTK1
Unknown aminotransferase
MTR
Met
MTN (LIKE1)
MTA
MAT1 (LIKE)
MAT2
MAT3
SAM
ACS1
ACS2
ACS3 (LIKE)
ACS7
ACS9 (LIKE)
ACC Synthase
ACC
ACO1 (LIKE)
ACO2
ACO3
ACO5
ACC Oxidase
2 H2O + HCN + CO2
Ethylene
Yang cycle gene
Biosynthesis gene
C)
ER Lumen
ER Membrane
Cytosol
Nucleus
EBF1/2 protein
EIN2-N
EIN2-C
EIL1
EIL2
EIN3
EIL3
Proteolytic cleavage
EBF1/2 mRNA
ORE1/2
ERF1
EIN2
ETP1/2
P
Ethylene-Induced Responses
Ethylene CH2=CH2
ERS1
ETR2
CTR1 & CTR1-LIKE
Ethylene
ETR1
RTE1
Senescence
RAN1
FYF 1 (LIKE)
FYF2/ SOC1
FYF3/ AGL19
FYF4/ AGL42

478

Figure 2 Updated genomic localization of ERGs and updated models of the ethylene pathway in *Cannabis sativa*. (A) Chromosomal positions of ethylene-related genes (ERGs) identified in *C. sativa* transcriptomes from Monthony et al. (2024) and expanded in the present study. Autosomal gene positions are based on the 'Pink Pepper' reference genome (NCBI, 2023); Pseudo-autosomal region (PAR) and non-recombining sex determination region (SDR) regions on the X and Y chromosomes follow Carey *et al.* (2024b). (B) Simplified model of the Yang cycle and ethylene biosynthesis pathway, updated from Monthony et al. (2024) to reflect gene presence in *C. sativa*. (C) Updated model of the canonical ethylene signaling pathway, including ER-localized receptors, CTR1-mediated EIN2 phosphorylation, and EIN2-C–dependent regulation of ethylene responses via EBF1/2, EIN3/EILs, ERF1, and FYFs. Color indicates subcellular localization (ER-bound: blue, cytosolic: orange, nuclear: light orange); arrowheads denote activation (pointed) or inhibition (blunt), in the presence (green) or absence (red) of ethylene. Dashed arrows indicating indirect or abbreviated steps. Single, grey dashed arrow indicates movement. A detailed review of ethylene biosynthesis and signaling pathways can be found in Binder (2020).

The newly available fully phased XY genome allowed us, for the first time, to report putative ERGs present in both the X and Y chromosomes, including those localized in the pseudoautosomal region (PAR) and the non-recombining sex-determination region (SDR; Figure 2A). Ortholog analysis identified six X-specific ERGs, all within the putative SDR region of the X chromosome. Additionally, four ERGs were detected in the X chromosome PAR, with homologs in the Y chromosome PAR. Notably, no Y-specific ERGs were identified. A complete list of genes present in the X and Y haplotypes of the Otto II genome can be found in Supplementary Table 13. Compared to our earlier analysis using the older cs10 genome assembly, which identified a single *MTN* gene, the improved ortholog resolution enabled by the Pink Pepper and Otto II genomes revealed two MTN-family genes. These were provisionally named *CsMTN* and *CsMTN-LIKE1*, based on sequence similarity to *Arabidopsis MTN1* and *MTN2*. *CsMTN* matched both *MTN1* and *MTN2*, while *CsMTN-LIKE1* showed weaker similarity to *MTN2* and had been annotated as a nucleosidase-like gene in the *C. sativa* reference genome (NCBI 2023; Supplementary Table 13).

Taken together, these new ERGs were integrated into an updated model for the Yang cycle, ethylene biosynthesis and signaling (Figure 2 B &C).

Low nucleotide diversity suggests ERGs are highly conserved in *C. sativa*

To explore genetic variation within key CsERGs, we characterized single nucleotide polymorphisms (SNPs), structural variants (SVs), and nucleotide diversity (θ_π) across the whole genome and 47 CsERGs. Variant calling on the genomes of XX and XY Deadly Kernel, La Rosca, and Panama Pupil V4 (n = 6 genomes) identified approximately 6.7 million polymorphic SNPs and ~78 thousand SVs relative to the *C. sativa* 'Pink Pepper' reference genome. Within ±5 kb regions of the 47 CsERGs, 8,670 SNPs and 98 SVs were detected (Supplemental Figure 2A). Of these, 3,611 SNPs and 29 SVs were located within CsERGs gene sequences and were further examined for potential functional impact. The majority of variants were found in intronic regions or the 3' and 5' UTRs, and were classified as having modifier impact (Supplemental Figure 2B&C). Among coding region variants, most SNPs were synonymous, although 114 caused missense mutations, and 13 high-impact variants (7 SNPs and 6 SVs) were identified (Supplemental Figure 2 D&E). Notably, LOC115719259 (*CsMAT2*), LOC115716986 (*CsFYF3*), and LOC115717309 (*CsFYF4*) exhibited a high density of SNPs, primarily within introns, consistent with their predominantly (>90%) intronic gene structure. Additionally, LOC115706236 (*CsCTR1-LIKE*) and LOC115702329 (*CsETR1*) also showed elevated SNP counts (>100 SNPs). Across these five highly polymorphic genes, the average nucleotide diversity was 7.21×10^{-3}, notably higher than the genome-wide average of 3.60×10^{-3} (Supplementary Table 14).

Across all CsERGs, the average nucleotide diversity was 2.85×10^{-3}, indicating lower diversity than the genome-wide estimate. This signal was even more pronounced when excluding the five highly polymorphic genes, with the remaining 42 CsERGs exhibiting an average nucleotide diversity of 2.33×10^{-3}. Interestingly, CsERGs located in sex chromosome subregions also displayed reduced variation: X-linked CsERGs within the SDR had an average nucleotide diversity of 1.77×10^{-3}, while those located in the pseudoautosomal region (PAR) showed the lowest diversity overall at 1.46×10^{-3}. The elevated SNP density observed in the five high-diversity genes may reflect underlying structural variants miscategorized during alignment.

ACC Accumulation Differs by Sex and Stage

Endogenous ACC levels were quantified in *C. sativa* leaves at vegetative (day 0) and flowering (day 1) stages across experimental groups (Supplemental Figure 3A and Supplementary Table 15). Estimated marginal means from the linear mixed-effects model revealed that ACC concentrations were significantly higher in XY Day 1 - IFF compared to XX Day 0 - FF and XX Day 1 - FF (Tukey's HSD, $\alpha = 0.05$). No other groups displayed significant differences in ACC levels. No significant change in ACC concentration was observed between pre- and post-flowering XY plants, regardless of treatment. Additionally, IMF exhibited intermediate ACC levels between male (XY) and female (XX) floral phenotypes. SAM quantification was below the level of quantification and is presented as presence/absence in Supplementary Table **15**.

Among all ERGs analyzed, CsCTR1-LIKE expression exhibited a strong and significant negative correlation with ACC concentration in XX Day 0 - FF ($\rho = -0.8$, $p \leq 0.001$). However, no

significant correlations were observed in other groups (Supplemental Figure 3B). Notably, all XY treatments exhibited weak positive correlations with CsCTR1-LIKE expression, suggesting a difference between CTR1-LIKE expression in XX and XY plants. Following STS treatment, IMF correlation remained strongly negative, while the control XX female flower exhibited only a weak correlation (Supplemental Figure 3B).

Transcriptomics and Network analysis

Time and sex-driven transcriptomic patterns in XX and XY plasticity

To understand the effect of sexual plasticity treatments on ERG expression over time and tissue-type, transcriptomes were obtained from leaves (day 0 and day 1) and immature flowers (day 14) across treated, and untreated XX and XY plants of the DK, LR and PP genotypes. This yielded 139 transcriptomes, comprising ~8 billion mapped reads with 24x coverage and high mapping quality (score = 103, insert size = 302 bp, Supplementary Table 10). PCA analysis found that the proportion of variance explained by the first two principal components increases over time (Figure 3A-C). At Day 0, PC1 and PC2 together account for 46.25% of the total variance (PC1: 29.07%, PC2: 17.18%). By Day 1, the combined variance explained increased to 61.94% (PC1: 41.66%, PC2: 20.28%), and at Day 14, it reached 74.05% (PC1: 49.41%, PC2: 24.64%). At day 0, PCA of ERG expression in untreated leaves showed a clear separation between XX and XY samples along PC1 (Figure 3A). The corresponding heatmap (Figure 3D) suggests that this clustering is driven by a subset of highly expressed ERGs in XX plants, including *CsCTR1/CTR1-LIKE*, *CsMTK1*, *CsFYF4/AGL42* and *CsACO3*.

Following photoperiod change and application of the sex-altering treatments, changes in ERG expression patterns were observed at day 1. An increased variance is observed among treated groups, notably ethephon-treated XY plants (IFF) which showed a sharp divergence from other treatments along both principal components (Figure 3B). The heatmap for day 1 (Figure 3E) highlights elevated expression of ethylene signaling genes in IFF plants, including *CsEBF1*, *CsERS1*, *CsRTE1*, *CsETR2* and *CsEBF2*.

By day 14, PCA of ERG expression in immature flowers reveals a partial overlap between IFFs and the FF controls tissues (Figure 3C). The heatmap (Figure 3F) shows two distinct blocks of floral organ concordant (FOC) gene expression –shared gene expression among flowers of the same phenotypic sex. A female-biased, FOC block of ERGs including genes from the Yang Cycle (*CsMAT2/3*, *CsMTK1* and *CsDEP1*), ethylene biosynthesis (*CsACS2* and *CsACS3-LIKE*) as well as ethylene signaling and signaling-adjacent genes (*CsFYF2*, *CsFYF4* and *CsCTR1-LIKE*) are clustered in the top rows (Figure 3F).

In contrast, male expression patterns were more complex. PCA indicated that MFs and IMFs remained distinct, with separation along both principal components (Figure 3C). The heatmap (Figure 3F) revealed both FOC gene expression and the presence of uniquely expressed ERGs (uERGs) in MFs. Male-biased ERGs included *CsMTN/MTN-LIKE1* (Yang Cycle), *CsACS1*, *CsACS7*, *CsACO5* (biosynthesis), and multiple ethylene signaling-related genes (*CsEBF1*, *CsEBF2*, *CsERF1*, *CsFYF3*, *CsRAN1*, *CsEIN3*, *CsEIN2*, *CsBPC2*). Additionally, a set of uERGs

was highly expressed only in MFs, including *CsARD2*, *CsMTI1*, *CsMAT1* (Yang Cycle), *CsACO2*, *CsACO1* (biosynthesis), and *CsETP1*, *CsETR2*, *CsORE1*, *CsORE2* (signaling).

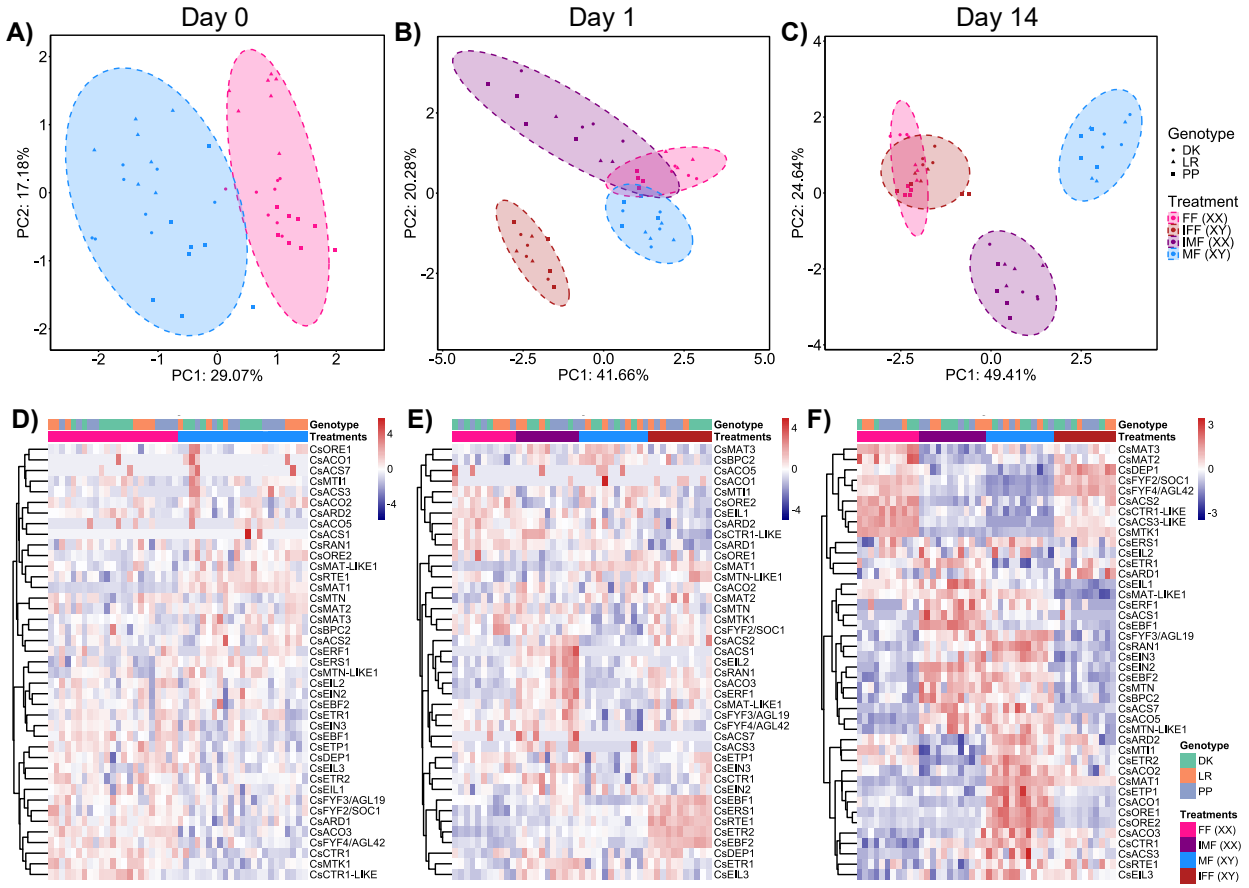

Figure 3 Principal Component Analysis (PCA) and heatmaps of 47 ERG expression across experimental time points and treatments. PCA was performed on batch-corrected variance-stabilized transformed (VST) counts of 47 ERGs. (A) Day 0 (pre-treatment, leaves); (B) Day 1 (post-treatment, leaves); (C) Day 14 (post-treatment, immature flowers). Each point represents an individual sample, and ellipses indicate the 95% confidence intervals for each group. Colors correspond to treatment groups, while symbols indicate cultivars (DK: Deadly Kernel, LR: La Rosca; PP: Panama Pupil V4). D-F) Heatmaps displaying expression patterns of 47 ERGs for each time point. Heatmap colors represent z-scores of gene expression, with rows corresponding to genes and columns to samples. The hierarchical clustering of genes (y-axis) was performed using Euclidean distance and complete linkage.

Network analyses reveal XX and XY-unique ERGs involved in sexual plasticity

The PCA suggesting distinct XX and XY ERG expression patterns in response to sexual plasticity treatments led us to construct two separate sex-specific gene co-expression networks. This allowed for the identification of modules specific to each genotypic sex without cross-sex effects influencing module detection. WGCNA network construction for XX and XY plants resulted in networks with 12 and 16 module Eigengenes (ME), respectively. Hierarchical clustering dendrograms (Supplemental Figure 4A & B) display the gene co-expression relationships within these sex-specific networks. Distinct clustering patterns and variations in module compositions, size and number were observed between the XX and XY networks.

Module-trait correlation analyses were performed independently for the XX and XY networks to identify modules significantly associated with treatment and specific time points (Supplemental Figure 4C & D). Priority was given to modules strongly correlated with treatment to identify gene clusters most responsive to the experimental conditions. In the XX network (Supplemental Figure 4C), five modules displayed significant correlations with treatment: MEbrown ($r = -0.89$), MEblack ($r = -0.52$), MEmagenta ($r = 0.54$), MEblue ($r = 0.66$) and MEred ($r = 0.71$). For the XY network (Supplemental Figure 4D), three modules surpassed the threshold for significant correlation with treatment: MEgrey ($r = 0.53$), MEpink ($r = 0.65$), and MEgreenyellow ($r = 0.5$).

From these treatment-associated modules, ERGs were extracted for further investigation, identifying 19 ERGs in the XX network, and 6 ERGs in the XY network, resulting in a total of 24 unique ERGs (Supplementary Table 16). To evaluate their functional significance within each

module, intramodular connectivity (kME) was calculated. The most highly connected gene in the XX network was *CsACO5* (kME = 0.96), while in the XY network, *CsERF1* exhibited the highest connectivity (kME = 0.93). Interestingly, *CsERF1* was the only gene present in both networks, with a kME of 0.95 in the XX network. All 24 ERGs were retained for subsequent differential gene expression analysis.

Differential expression analysis reveals 14 candidate sexual plasticity ERGs

To refine the candidate ERGs involved in sexual plasticity, we conducted differential gene expression (DGE) analysis on the 24 ERGs identified from treatment correlated XX and XY WGCNA modules. Contrasts were set between treated and untreated samples of the same genotypic sex at time points following sexual plasticity treatment (Day 1 and Day 14), and genes were considered significantly differentially expressed if $|\log_2(\text{Fold Change})| \geq 1$ and adjusted p-value ≤ 0.05 across all three genotypes. Of the initial 24 ERGs, 14 met these filtering criteria (grey highlighted genes in Supplemental Figure 5). The resulting refinements yielded a candidate ERG list including those most likely to play a role in ethylene-mediated sexual plasticity in *C. sativa* (Table 2).

Table 2 Candidate sexual plasticity ERGs in XX and XY *C. sativa*. Candidate ERG filtration included those identified with a significant WGCNA correlation between module and treatment (r ≥ 0.5; p-adjust ≤ 0.05) followed by a filtration using differential gene expression (DGE). DGE was conducted intra-sex on day 1 or day 14 retaining only those genes which were significantly (p-adjust ≤ 0.05) differentially expressed across all 3 tested genotypes. Log_2FC values denoted by a * meeting filtration criteria for significant differential expression (p-adjust ≤ 0.05; $|\log_2\text{FC} \geq 1|$; in 3 genotypes).

Sex Association	**CsERG**	**Locus ID (LOC)**	**Pathway**	**Intramodular Connectivity (kME)**		**Differential Expression ($\log_2$FC)**			
						IMF (XX) vs. FF (XX)		**IFF (XY) vs MF (XY)**	
				XX Network	**XY Network**	Day 1	Day 14	Day 1	Day 14

XX/XY	*MTN*‡	115704327	Yang Cycle	0.73	0.67	0.02	1.14*	0.27	-1.01*
	MTN-LIKE1‡	133033195	Yang Cycle	0.79	0.73	-0.07	1.17*	0.20	-1.10*
	ACO3	115699412	Biosynthesis	-0.77	0.81	2.48*	0.27	1.68*	-0.61
	EBF1†	115720532	Signaling	-0.83	-0.63	0.22	1.56*	1.71*	-0.21
	FYF2/SOC1	115706939	Adjacent	-0.83	-0.95	-0.13	-1.22*	0.24	2.60*
	FYF4/AGL42	115717309	Adjacent	-0.82	-0.78	0.06	-1.69*	0.10	3.93*
XX	*MTK1*‡	115703014	Yang Cycle	-0.74	0.28	-0.01	-1.47*	0.32	0.90
	MAT2	115719259	Yang Cycle	0.81	0.48	0.12	-2.48*	0.11	0.38
	ACS1	115704849	Biosynthesis	0.94	0.38	6.03*	1.90*	0.17	-0.35
	ACS2	115717044	Biosynthesis	-0.47	-0.43	0.56	-1.72*	1.30*	0.82
	ACO5†	115699408	Biosynthesis	0.96	0.92	-0.23	4.17*	-0.01	-1.77
	ERF1	115723050	Signaling	0.95	0.93	5.37*	0.44	1.40	-1.20
XY	*EBF2*	115724585	Signaling	0.73	0.61	0.43	0.65	1.33*	-0.63
	RTE1‡	115707134	Signaling	0.65	0.73	0.05	0.03	1.50*	-0.10

† indicates that the gene is present only on the X chromosome

‡ indicates a gene is present on the X and Y chromosome

From the 14 candidate ERGs, six met the criteria for association with sexual plasticity in both XX and XY sex changed plants, a further six were associated with XX plants only and two with XY plants (Table 2). Within the XX and XX/XY-associated ERGs, there was representation from all pathways including: Yang cycle (e.g., *MTN*, *MAT2*), ethylene biosynthesis (e.g., *ACS1*, *ACO5*), signaling (e.g., *EBF1*, *ERF1*), and signaling adjacent regulatory pathways (e.g., *FYF4/AGL42*). In contrast, the XY-associated ERGs were primarily limited to signaling components (*EBF2*, and *RTE1*), perhaps reflecting the signaling response from the ethephon-induced sex change.

To identify temporal patterns underlying ethylene-induced sexual plasticity, we examined the differential expression of ethylene-related genes (ERGs) at two stages: in mature leaves immediately following treatment and photoperiod change (day 1) and in immature inflorescences during active sexual phenotype transition (day 14). Genes strongly associated with day 1 by WGCNA and/or differential expression analysis were classified as plasticity initiators, while those associated with day 14 were classified as plasticity stabilizers (Figure 4).

In XX plants, three differentially expressed ERGs were significantly associated with plasticity initiation and ten associated plasticity stabilization (Table 2). Initiators included *ERF1* ($\log_2$FC = 5.37) and *ACO3* ($\log_2$FC = 2.48; Figure 4A), which were significantly upregulated in IMFs compared to FFs at day 1, suggesting early activation of ethylene biosynthesis and signaling pathways. By day 14, several ERGs displayed substantial differential expression, including strong upregulation of *ACO5* ($\log_2$FC = 4.17; Figure 4B) and *EBF1* ($\log_2$FC = 1.56), as well as moderate upregulation of the Yang cycle-associated genes *MTN* ($\log_2$FC = 1.14; Figure 4B) and *MTN-LIKE1* ($\log_2$FC = 1.17). In contrast, *MAT2* exhibited marked downregulation ($\log_2$FC = –2.48). *ACS1* was the only ERG significantly differentially expressed at both timepoints in XX plants, with strong upregulation at day 1 ($\log_2$FC = 6.03) and sustained, though reduced, expression at day 14 ($\log_2$FC = 1.90), suggesting a role in both the initiation and stabilization of sexual plasticity (Figure 4C).

In XY plants, five ERGs were classified as initiators and four as stabilizers (Table 2). Two initiators, *EBF2* ($\log_2$FC = 1.33) and *RTE1* ($\log_2$FC = 1.50), were differentially expressed only in masculinized XY plants and did not show corresponding changes in XX plants. Among stabilizers,

FYF2 and *FYF4* were strongly upregulated during the phenotypic transition observed at day 14 (log_2FC = 2.60 and 3.93, respectively). *MTN* and *MTN-LIKE1*, which were upregulated in XX plants, were downregulated in XY plants (log_2FC = –1.01 and –1.10, respectively; Figure 4B).

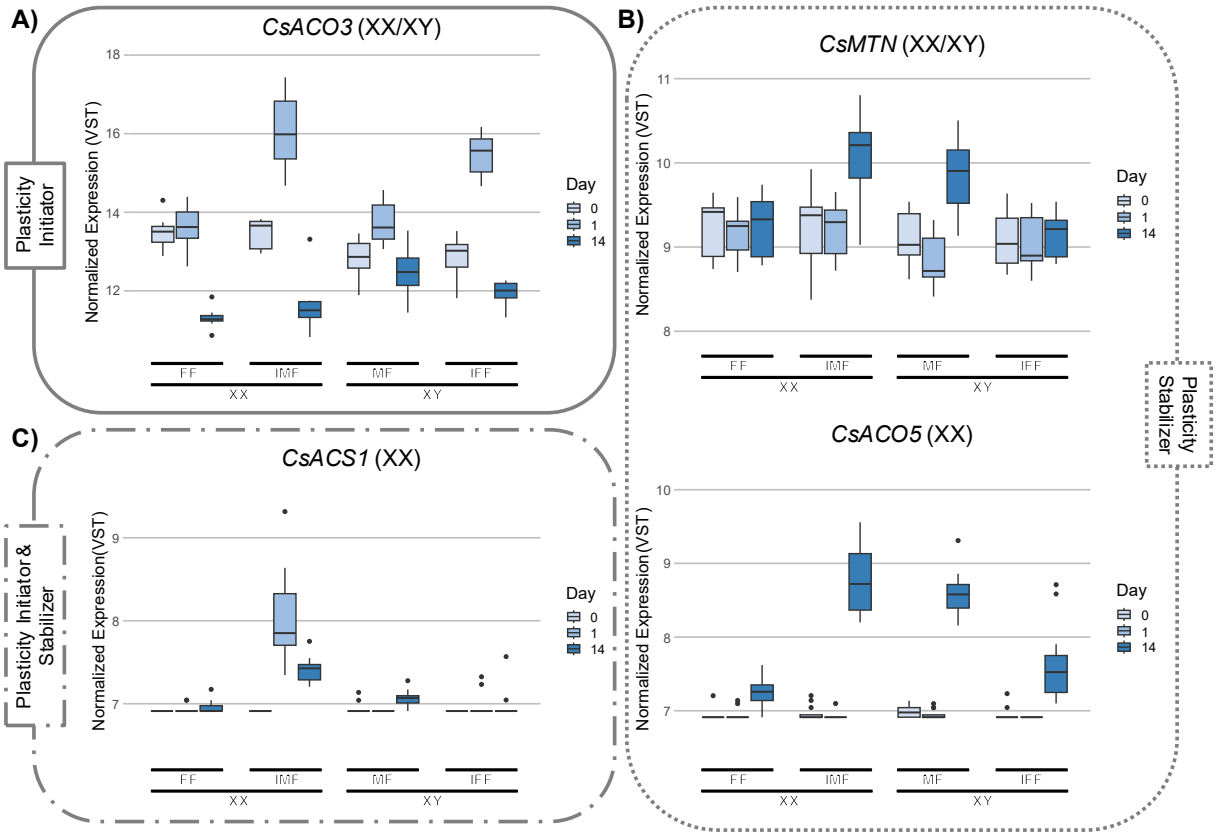

Figure 4 Representative VST normalized ERG RNA expression profiles for sexual plasticity initiators (A & C) and plasticity stabilizer genes (B), as identified using WGCNA and DGE filtration. Brackets next to names indicate chromosomal sex of plants where a significant effect of the gene on plasticity was identified.

The candidate ERGs were used to create a working model for the temporal control of ethylene-regulated sexual plasticity (Figure 5). This model incorporates plasticity initiators and plasticity stabilizers, highlighting their dynamic changes in sex- and treatment-specific expression profiles

over time. Importantly, candidate ERGs critical to sexual plasticity regulation appear consistently at pathway bottlenecks, where alternate signaling routes are absent or limited. Key examples include *MTN* and *MTK1* at the initiation of the Yang cycle, *ACS1/2* and *ACO3/5* in the biosynthesis pathway (Figure 2B & Figure 5), and *EBF1/2* and *ERF1* in downstream signaling (Figure 2C & Figure 5).

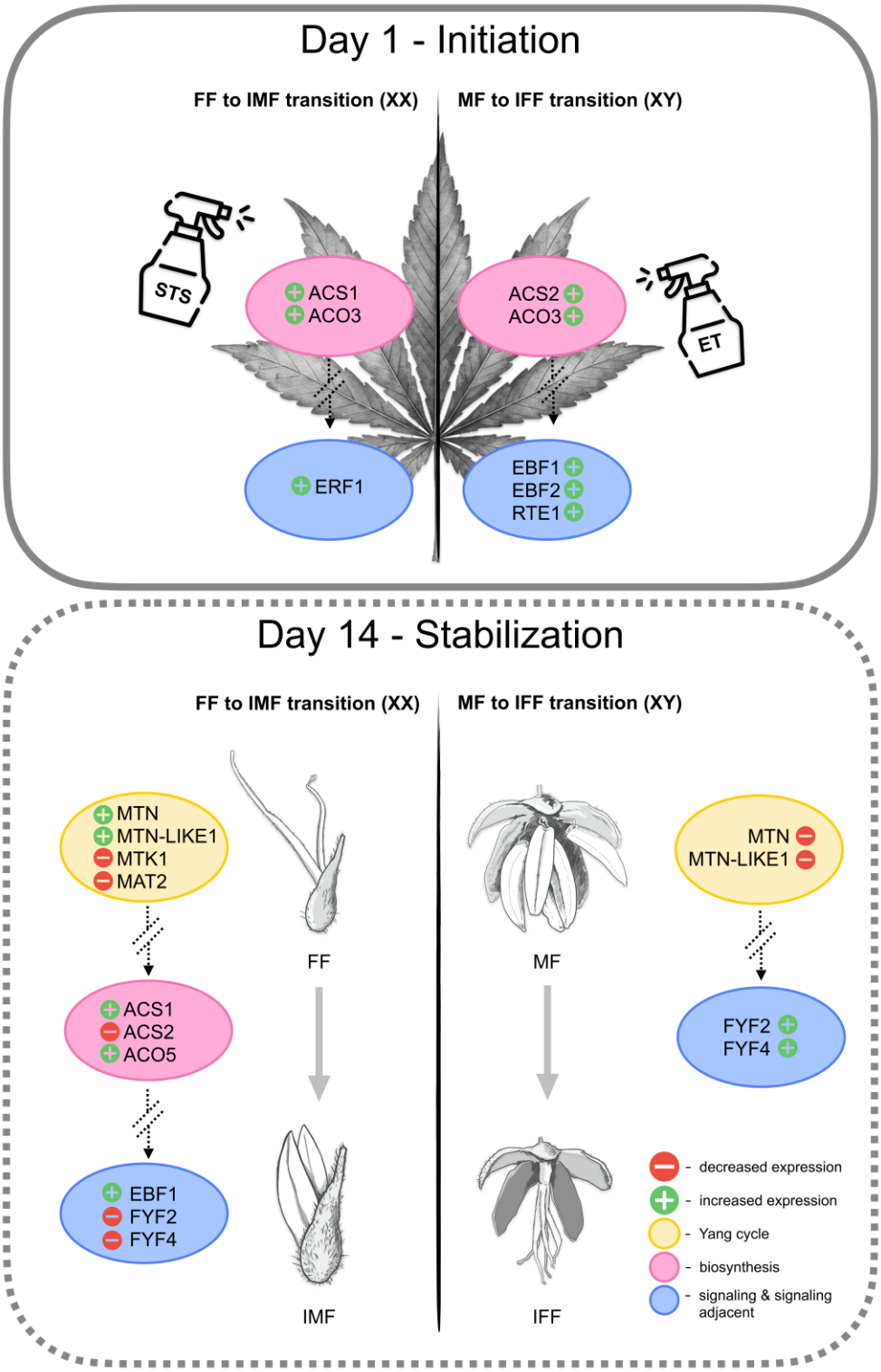
Day 1 - Initiation
FF to IMF transition (XX)
MF to IFF transition (XY)
STS
ACS1
ACO3
ACS2
ACO3
ET
ERF1
EBF1
EBF2
RTE1
Day 14 - Stabilization
FF to IMF transition (XX)
MF to IFF transition (XY)
MTN
MTN-LIKE1
MTK1
MAT2
FF
ACS1
ACS2
ACO5
EBF1
FYF2
FYF4
IMF
MF
MTN
MTN-LIKE1
FYF2
FYF4
IFF
- decreased expression
- increased expression
- Yang cycle
- biosynthesis
- signaling & signaling adjacent

673

Figure 5 Working model of ethylene-induced sexual plasticity in Cannabis sativa. This model proposes two phases of ethylene-mediated sexual plasticity: initiation and stabilization, each marked by distinct patterns of ethylene-related gene (ERG) expression. Initiation (Day 1) is characterized by a broad upregulation of ethylene biosynthesis and signaling genes in both induced male flowers (IMFs, XX) and induced female flowers (IFFs, XY), relative to their respective untreated controls (FF and MF). During the stabilization phase (Day 14), IMF and IFF plants begin to diverge in the expression of key ERGs that maintain their altered floral phenotypes. These include genes up- and down-regulated across the Yang cycle, ethylene biosynthesis, ethylene signaling, and signaling-adjacent pathways. Expression changes are represented by directional symbols (green "+" for upregulation, red "–" for downregulation) based on $\log_2$ fold change ($\log_2$FC) values relative to untreated controls. The FF to IMF transition (XX) refers to gene expression changes in IMFs compared to untreated FFs, and the MF to IFF transition (XY) refers to gene expression changes in IFFs compared to untreated MFs.

Discussion

Sexual plasticity, the capacity of a plant to shift its phenotypic sex from its baseline genetic sex in response to internal or external cues, is a phenomenon observed in many monoecious and dioecious species (Lin *et al.*, 2016; Cossard & Pannell, 2021; Käfer *et al.*, 2022). In cannabis, strong evidence exists for ethylene-mediated sexual plasticity (Galoch, 1978; Moon *et al.*, 2020; Adal *et al.*, 2021). Ethylene is a PGR that plays a role in many plant processes, including playing a central role in sex determination in most Cucurbitaceae species (Chen *et al.*, 2016b; Li *et al.*, 2021). Beyond the Cucurbitaceae family, however, evidence for ethylene's role as a key regulator of sex determination and sexual plasticity in dioecious plants is relatively rare. One notable case is in *C. sativa*, where ethylene inhibitors have been widely used to induce female-to-male conversion (Kurtz *et al.*, 2020), while ethylene-releasing compounds (e.g., ethephon) trigger the opposite phenotypic transition, from male to female (Moon *et al.*, 2020).

Given the highly heterozygous nature of *C. sativa*, it is crucial to conduct multi-genotype studies to accurately capture species-wide biological responses (Page *et al.*, 2021; Monthony *et al.*, 2021b). Therefore, in this study, we comprehensively investigated ethylene-induced sexual plasticity across three distinct cannabis genotypes, demonstrating a conserved phenotypic response in both XX and XY plants (Table 1), achieving inflorescence sex change rates comparable to previous reports (Lubell & Brand, 2018; Moon et al., 2020). This broad responsiveness supports the hypothesis of a conserved group of ERGs and a species-wide mechanism underlying ethylene-mediated sexual plasticity.

While ERGs are broadly distributed throughout the genome, we identified 12 ERGs located on the sex chromosomes of *C. sativa*, with six genes in the pseudoautosomal region (PAR) and six within the non-recombining SDR of the X chromosome (Figure 2A). Notably, no ERGs were found within the Y-linked SDR. Although suppressed recombination in the SDR is expected to reduce nucleotide diversity compared to the PAR (Otto *et al.*, 2011), our analysis revealed that ERGs located in the PAR displayed even lower nucleotide diversity ($\theta\pi = 1.46 \times 10^{-3}$) compared to those in the X-linked SDR ($\theta\pi = 1.77 \times 10^{-3}$), with both regions showing diversity levels below the autosomal ERG average ($\theta\pi = 3.23 \times 10^{-3}$). This pattern provides evidence for strong purifying selection acting on functionally critical PAR genes, particularly *CsMTK1*, *CsRTE1*, and *CsMTN*/*MTN-LIKE1*, which lack autosomal homologs for their respective enzymatic roles within the ethylene biosynthetic pathway.

MTN plays a key role recycling methylthioadenosine (MTA)—a byproduct of the first committed step in ethylene biosynthesis. In the present study *CsMTN* and *CsMTN-LIKE1* were identified within a WGCNA module strongly correlated (r = 0.66) with sexual plasticity treatment in XX plants. Both genes showed high module membership in this network (kME = 0.73 and 0.79, respectively), supporting their centrality in the transcriptional response to masculinization. Differential expression analysis indicated significant upregulation of *CsMTN* and *CsMTN-LIKE1* in IMFs relative to untreated XX controls ($\log_2$FC = 1.14 and 1.17, respectively). In XY plants, IFFs, had significant downregulation of *CsMTN* and *CsMTN-LIKE1* ($\log_2$FC = -1.01 and -1.10) compared to untreated XY (MF) controls. These findings align with our previous study showing a male phenotype-biased expression of *MTN* (Monthony *et al.*, 2024) and with Borin *et al*. (2024), who reported high *CsMTN* expression in MF and IMFs. Functional analyses in Arabidopsis revealed that *MTN* is critical for male reproductive development, as *mtn1-1 mtn2-1* double mutants exhibit indehiscent anthers and malformed pollen grains (Waduwara-Jayabahu *et al.*, 2012). In the dioecious species *Amborella trichopoda*, transcriptomic analyses of immature flowers revealed differential expression of *AmbMTN* by sex, with higher expression in female tissues (Carey *et al.*, 2024a).

Elevated *CsMTN* transcript levels in phenotypic male flowers, suggests a role in ethylene-induced sexual plasticity; however, *CsMTN* downregulation in ethephon-treated XY plants would suggest that it is not directly regulated by ethylene in *Cannabis*. Instead, *MTN* may be developmentally or metabolically modulated to sustain the biosynthetic demands linked with male floral identity. This interpretation aligns with findings in rice, where *OsMTN* transcript and enzyme activity increase alongside ethylene levels during submergence, but were shown to not be ethylene-induced

(Rzewuski *et al.*, 2007). Similarly, in Arabidopsis, it has been demonstrated that Yang cycle genes like *MTN* are essential for sustained ethylene biosynthesis, but not ethylene-responsive (Bürstenbinder *et al.*, 2007). Ethylene-responsive Yang cycle gene expression does occur in other species such as tomato (van de Poel *et al.*, 2012), suggesting a species-specific evolutionary relationship between ethylene signaling and Yang cycle regulation. Given these regulatory nuances, we next examined *CsMTK1*, another Yang cycle gene, to further explore the role of methionine recycling during sexual plasticity.

CsMTK1, another Yang cycle candidate sexual plasticity gene is localized on the PAR of *C. sativa* (Figure 2A). *CsMTK1* catalyzes the phosphorylation of 5-methylthioribose (MTR), the product of of MTN activity, to yield 5-methylthioribose-1-phosphate (Figure 2B). To date, a single *MTK* has been identified in *C. sativa*, consistent with *A. thaliana*, *Plantago major* L. and several other plant species (Pommerrenig *et al.*, 2011; Chen *et al.*, 2025). While *CsMTN* and *CsMTN-LIKE1* showed strong connectivity within WGCNA modules associated with sexual plasticity in XX and XY networks, *CsMTK1* displayed XX-specific expression. In the XX network, it was negatively correlated with the plasticity module (*kME* = –0.74) and exhibited low connectivity in the XY network (*kME* = 0.28), suggesting a more limited role in male-to-female transitions. *CsMTK1* transcripts were significantly downregulated in IMFs ($\log_2$FC = –1.47) compared with FFs, and showed no significant change between IFFs and MFs ($\log_2$FC = 0.90). This temporal and tissue-specific downregulation—only observed in flowers at Day 14—suggests that CsMTK1 is not directly regulated by ethylene but may instead be developmentally modulated. This interpretation aligns with findings in *Arabidopsis* and *rice*, where MTK expression is critical for SAM recycling and ethylene biosynthesis under sulfur-limited conditions, but is not transcriptionally induced by

ethylene (Bürstenbinder *et al.*, 2007; Rzewuski *et al.*, 2007). By contrast, MTK expression is ethylene-responsive in climacteric species such as *tomato* and *cucumber*, pointing to a species-specific regulatory architecture (van de Poel *et al.*, 2012; Chen *et al.*, 2025). In *Cannabis*, these patterns support a functional decoupling between *CsMTN* and *CsMTK1* during sexual plasticity, wherein MTA cleavage via MTN is prioritized while methionine recycling through MTK1 is developmentally downregulated. Supporting this, *CsMTK1* exhibited elevated nucleotide diversity ($\pi = 4.58 \times 10^{-3}$), higher than both the PAR ERG average and genome-wide mean, suggesting relaxed purifying selection relative to *CsMTN*. Together, the gene expression and nucleotide diversity data suggest that *MTK1* may be dispensable for ethylene-mediated sex change in *Cannabis*.

In addition to the aforementioned PAR-linked Yang cycle genes, we identified *CsMAT2*, an autosomal Yang cycle gene located on chromosome 2 (Figure 2A), encoding methionine adenosyltransferase (MAT or SAMS), which catalyzes the formation of S-adenosylmethionine (SAM)—the precursor to ACC and a central metabolite in ethylene biosynthesis. *CsMAT2* exhibited strong connectivity within the XX network (kME = 0.81) but weaker connectivity in the XY network (kME = 0.48). It was significantly downregulated in IMFs compared to FFs at Day 14 ($\log_2$FC = –2.48), a developmental window that coincides with the early stages of pollen maturation in IMFs (DiMatteo *et al.*, 2020 & Figure 1). Furthermore, *CsMAT2* displayed the highest nucleotide diversity among all ERGs analyzed ($\pi = 5.99 \times 10^{-3}$), exceeding the genome-wide average (Supplementary Table 14). This elevated diversity could reflect relaxed selection on *CsMAT2* due to redundancy within the *MAT* gene family—four *MAT/SAMS* genes are present in the *C. sativa* genome (Figure 2B)—a pattern also observed in tomato where distinct *SlMAT*

paralogs are expressed in a tissue- and stage-specific manner during ethylene-mediated fruit ripening (van de Poel *et al.*, 2012). This suggests that *CsMAT2* may represent a functionally specialized member of the *MAT* family in cannabis, with a potential role in early floral development that merits further investigation.

In both *Arabidopsis* and *rice*, disruption of *MAT* genes has been shown to impair pollen tube growth, reduce male fertility, and compromise seed set (Chen *et al.*, 2013, 2016c), highlighting developmental functions beyond SAM provision. While our study does not directly assess pollen viability, the observed downregulation of *CsMAT2* during early pollen development in IMFs raises the possibility of a functional role in male gametophyte development. This is particularly relevant given the frequently reported poor pollen quality in STS-induced male flowers in *Cannabis sativa* (Lubell & Brand, 2018; DiMatteo *et al.*, 2020). Notably, in pumpkin fruit, a long non-coding RNA has been shown to stabilize SAMS protein, promoting fruit development via ethylene biosynthesis (Tian *et al.*, 2024), illustrating how *MAT* regulation can directly modulate ethylene-dependent developmental outcomes. Future studies investigating *CsMAT2* function in the context of floral reprogramming may help clarify whether its transcriptional modulation contributes to impaired pollen development during ethylene-induced sexual plasticity.

The final candidate ERG located in the PAR is *CsRTE1*, a known negative regulator of ethylene signaling. Unlike the Yang cycle genes discussed above, which may play a role in modulating the biosynthetic capacity of the pathway, *CsRTE1* acts in the ethylene signaling pathway, appearing as a responsive gene rather than a driver of sexual plasticity. In our study, *CsRTE1* was

significantly upregulated in XY leaf tissue one day after ethephon treatment (Day 1 IFFs), a pattern not observed in treated XX plants. This response is consistent with previous findings in *Arabidopsis*, where *RTE1* is induced by ethylene and functions in a feedback loop to stabilize the ETR1 receptor and attenuate downstream signaling (Resnick *et al.*, 2006). The transient upregulation of *CsRTE1* in XY plants may reflect a mechanism for buffering early ethylene signaling—in this case in response to ethephon treatment—and preventing an overactivation of the autocatalytic ethylene biosynthesis loop. Supporting this, ACC concentrations in Day 1 IFFs were not significantly elevated compared to untreated XY plants (Supplemental Figure 3), suggesting that ethephon application does not trigger a runaway ethylene biosynthesis response within first 24 hours following ethephon treatment. Instead, *CsRTE1* may help modulate the ethylene response during the early reprogramming phase, maintaining signaling homeostasis as phenotypic feminization is initiated.

All six X-specific CsERGs on the SDR have homologs elsewhere in the genome (Figure 2A) and are either involved in ethylene biosynthesis (*CsACS3-LIKE* and *CsACO5*) or signaling (*CsETR1*, *CsCTR1*, *CsEBF1*, and *CsEIL1*). Among these, *CsACO5* and *CsEBF1*, were identified as candidate regulators of sexual plasticity (Table 2). *CsEBF1* and its autosomal counterpart, *CsEBF2*, encode F-box proteins that target the *EIN3/EIN3-LIKE* (*EIL1-3*) family of transcription factors for proteasomal degradation, serving as key negative regulators of ethylene signaling in the absence of hormone (Binder, 2020). In *Arabidopsis*, *EBF1/2* mRNA levels are typically suppressed following ethylene exposure via EIN2-C–mediated targeting of EBF1/2 mRNAs to processing bodies for degradation (An *et al.*, 2010; Binder, 2020). Surprisingly, both cannabis homologs were upregulated in ethephon-treated IFFs at Day 1 (EBF1 $\log_2$FC = 1.71; EBF2 $\log_2$FC = 1.33),

suggesting that their transcriptional regulation may diverge from the canonical Arabidopsis model. By Day 14, *CsEBF1* was also significantly upregulated in IMFs, a pattern not shared by *CsEBF2*. While this late-stage expression may imply a role in stabilizing the masculinized phenotype through suppression of ethylene signaling, the mechanism remains unclear. Considering the post-transcriptional regulation of *EBF1/2* reported in other species, it is uncertain whether the observed transcript accumulation reflects a regulatory feedback loop, a compensatory response, or unrelated developmental dynamics captured in our sampling window. Notably, *EBF1* is located on the SDR of the X chromosome, and while its spatial localization may contribute to XX-specific regulation, further work is needed to determine whether its sustained upregulation reflects a sex-linked regulatory function or a broader role in floral development under ethylene-modulated conditions. To better understand the downstream consequences of altered ethylene signaling in our dataset, we next examined CsERF1, a transcriptional response factor directly regulated by EIN3/EIL1 and a key integrator of ethylene-mediated developmental reprogramming.

ERF1, a central transcriptional activator in the ethylene signaling pathway, acts downstream of *EIN3* and *EIL1* to mediate broad ethylene responses through direct activation of GCC-box-containing target genes (Solano *et al.*, 1998; Binder, 2020). While not previously associated with sex determination, its well-documented role in ethylene-mediated developmental reprogramming makes it a plausible candidate for involvement in sexual plasticity. In our dataset, *CsERF1* was strongly upregulated in STS-treated XX plants at Day 1 (IMFs vs FFs; $\log_2$FC = 5.37) and exhibited the highest kME values of all candidate genes in both the XX (0.95) and XY (0.93) WGCNA networks, indicating tight integration with other genes responsive to sex change treatments. Although the IFF vs MF contrast in XY plants showed a $\log_2$FC of 1.40, this effect did

not meet our criteria for statistical significance due to genotype-level variability (Supplemental Figure 5). Nevertheless, this trend suggests that *CsERF1* may be responsive to ethylene exposure across both sexes, with a potentially conserved role in reprogramming floral identity. Taken together, these findings support a role for *CsERF1* as an early transcriptional integrator in ethylene-mediated sexual plasticity—particularly in XX plants—with suggestive evidence for broader involvement that warrants further investigation.

CsACO5, an X-linked gene with no Y copy, emerged as a compelling candidate for the stabilization of male floral identity during sexual plasticity, based on its strong and consistent upregulation in IMFs. Despite being X-linked, *CsACO5* levels are nearly identical in XY MFs and XX IMFs by day 14, implying regulation by the male-flower program, not chromosome count. At day 14, *CsACO5* expression was markedly upregulated in IMFs compared to the untreated FFs, with a $\log_2$FC of 4.17. Normalized *CsACO5* expression in MFs was comparable to IMFs, while IFFs exhibited reduced expression levels like those in FFs (Figure 4B), although the magnitude of this reduction in IFFs was genotype dependent (Supplemental Figure 5E). In all samples, *CsACO5* remains low at Day 0 and Day 1 (Figure 4B). Our findings associating *CsACO5* with masculinization of XX plants are consistent with Borin *et al*. (2024) and Monthony *et al*. (2024), both of whom reported elevated *CsACO5* expression in IMFs compared to FFs. Together, this supports a model in which *CsACO5* contributes to floral masculinization by stabilizing male identity during flower development.

Although ethylene is typically associated with feminization in dioecious species, studies in cucumber and melon have shown that disruption of specific *ACO* genes can lead to sex reversion and reduced ethylene production, underscoring the context-dependent roles of *ACO* enzymes in sex expression. Rather than initiating plasticity, *CsACO5* may function as a "stabilizer" that fine-tunes ethylene biosynthesis in developing male flowers. Supporting this, we observed that in immature floral tissues, LOC115706939 (*CsFYF2*) and LOC115717309 (*CsFYF4*)—predicted orthologs of Arabidopsis *FOREVER YOUNG FLOWER* (*FYF*) genes (Monthony *et al.*, 2024)—are consistently upregulated in phenotypically female flowers (FFs and IFFs). Similarly, Shi *et al*. (2024a) reported elevated LOC115706939 (annotated as *CsSOC1*) expression in female meristems and flowers, bolstering our observation of *FYF2* upregulation in day 14 female inflorescences. In contrast, these *CsFYF2/4* were significantly downregulated in MFs and IMFs (Table 2), with the shorter developmental lifespan of male cannabis inflorescences compared to female ones (Shi et al., 2024a). Taken together, these dynamics support a model in which ethylene-related genes act in a temporally structured manner during sexual plasticity, with early "initiators" like *CsACO3* triggering reprogramming and later "stabilizers" such as *CsACO5* consolidating male floral identity, while *CsFYF2* and *CsFYF4* modulate sex-specific senescence trajectories.

The final two candidate ERGs examined in this study, *CsACS1* and *CsACS2*, encode ACC synthase enzymes that catalyze the conversion of S-adenosylmethionine (SAM) to 1-aminocyclopropane-1-carboxylic acid (ACC), a key regulatory step in ethylene biosynthesis (Binder, 2020). Both genes were differentially expressed at Day 1, suggesting early transcriptional responsiveness to sex-change induction. *CsACS1* was strongly upregulated in STS-treated XX plants (IMFs) at Day 1 ($\log_2$FC = 6.03) and remained elevated at Day 14 ($\log_2$FC = 1.90), indicating a role in initiating

and possibly stabilizing masculinization (Table 2 & Figure 5). Normalized expression data showed a sharp spike in *CsACS1* expression at Day 1 in IMFs (Figure 4C), accompanied by a modest increase in ACC concentration (Supplemental Figure 3)—supporting its role as a plasticity-associated ethylene biosynthesis gene. Across all other tissues and treatments, including MFs and IFFs, *CsACS1* remained minimally expressed.

In contrast, *CsACS2* displayed a broader and less clearly sex- or treatment-specific pattern. In XY plants, *CsACS2* was upregulated following ethephon treatment at Day 1 ($\log_2$FC = 1.30), and downregulated in IMFs by Day 14 ($\log_2$FC = –1.72), reaching levels similar to MFs. However, the magnitude of these changes was comparatively small. Normalized expression showed that *CsACS2* expression was distributed across multiple tissue types and timepoints, including elevated expression in IFFs and Day 1 MFs—suggesting a more constitutive role in ethylene production. Previous studies have similarly reported variable *CsACS2* expression. Our previous study of ERGs found higher *CsACS2* expression in FFs compared with IMFs and MFs (Monthony *et al.*, 2024), while Borin *et al.* (2024) found no significant expression differences across FF, MF, and IMF flower tissues at Day 14 using qRT-PCR. These conflicting results may reflect tissue-type, developmental stage, or genotype-specific variation rather than a direct role in sexual plasticity. In other plant species, such as cucurbits and tomato, members of the ACS gene family show tissue- and stage-specific expression, with functionally distinct roles despite similar enzymatic activity (Van de Poel *et al.*, 2014; Boualem *et al.*, 2015). *CsACS2* may follow a similar pattern in *C. sativa*, highlighting the need for finer-resolution temporal and tissue-specific analyses to clarify its function.

Despite the sharp transcriptomic induction of *CsACS1* and *CsACS2* following sex-change treatments, this response was not fully mirrored in the measured ACC concentrations. For example, Day 1 IMFs showed the largest transcriptional increase in *CsACS1* ($\log_2$FC = 6.03) relative to FFs, yet ACC levels remained similar between these groups (Supplemental Figure 3). In contrast, IFFs exhibited the highest ACC concentration of all groups, despite a more modest *CsACS2* induction ($\log_2$FC = 1.30), aligning better with expectations. However, this apparent disconnect between ACS expression and ACC accumulation is consistent with previous findings in tomato, where tissues producing the most ethylene—such as the pericarp—had relatively low ACC content and ACS activity, while high ACC levels were observed in tissues with limited ethylene production (Van de Poel *et al.*, 2014). These discrepancies have been interpreted as evidence for tight spatial and temporal regulation of ACC metabolism and transport, as well as the rapid conversion of ACC to ethylene in actively ripening or differentiating tissues. In our study, this could mean that the elevated ACC levels observed in IFFs may reflect a lag between biosynthetic induction and ACC turnover, or potentially a localized ethylene amplification loop triggered by exogenous ethephon. Together, these findings suggest that ACC concentrations alone are not sufficient to infer ethylene biosynthetic activity, particularly during rapid transcriptional reprogramming. Instead, they highlight the complex interplay between transcriptional regulation, enzyme activity, ACC catabolism, and tissue-specific ethylene flux. Further work integrating spatial transcriptomics and enzyme activity profiling may be needed to clarify how *CsACS1* and *CsACS2* contribute to ethylene flux during cannabis sex change.

Our comprehensive investigation of ethylene-mediated sexual plasticity in *Cannabis sativa* highlights the complex interplay between genetic sex, ethylene signaling, and developmental

timing. Despite similar phenotypic outcomes from sexual plasticity treatments, by leveraging transcriptomics, metabolomics, and genomic analyses across multiple genotypes, we identified both conserved, sex- and time-specific ERGs underlying sexual reprogramming. Temporally, we observed distinct phases of ERG expression, identifying early responsive genes likely acting as plasticity initiators (e.g., *CsACO3*, *CsERF1*) plasticity stabilizers (*CsACO5*, *CsACS2*), or in the case of *CsACS1*: both (Figure 4). Additionally, our findings suggest the existence of sex-specific regulatory mechanisms, with certain ERGs showing strong responses predominantly in XX (e.g., *CsMAT2*, *CsMTN*, *CsMTK1*) or XY contexts (e.g., *CsRTE1*, *CsEBF2*). These insights have led us to a proposed a working model for understanding ERG-mediated sexual plasticity in cannabis (Figure 5), while also providing a robust framework for future sexual plasticity research.

Statements and Declarations

The authors have no competing interests to declare. The authors gratefully acknowledge the support of the Natural Sciences and Engineering Research Council (NSERC) of Canada. ASM has also been supported by a NSERC Canada Vanier Graduate Scholarship.

Data availability statement

All raw transcriptomic data will be made available on the NCBI sequence read archive (SRA) upon publication of this manuscript.

Acknowledgements

The authors would like to thank Christian Otis and Brian Boyle at the Université Laval Genomic Analysis Platform (PAG) for their invaluable counsel on RNA extraction, and Hélène Martin for her help sexing plant materials used in this study.

References

Adal AM, Doshi K, Holbrook L, Mahmoud SS. **2021**. Comparative RNA-Seq analysis reveals genes associated with masculinization in female Cannabis sativa. *Planta* **253**: 1–17.

Altschul SF, Gish W, Miller W, Myers EW, Lipman DJ. **1990**. Basic local alignment search tool. *Journal of Molecular Biology* **215**: 403–410.

An F, Zhao Q, Ji Y, Li W, Jiang Z, Yu X, Zhang C, Han Y, He W, Liu Y, *et al.* 2010. Ethylene-induced stabilization of ETHYLENE INSENSITIVE3 and EIN3-LIKE1 is mediated by proteasomal degradation of EIN3 binding F-box 1 and 2 that requires EIN2 in arabidopsis. *Plant Cell* **22**: 2384–2401.

Anand L, Rodriguez Lopez CM. **2022**. ChromoMap: an R package for interactive visualization of multi-omics data and annotation of chromosomes. *BMC Bioinformatics* **23**: 1–9.

Anger N, Fogliani B, Scutt CP, Gâteblé G. **2017**. Dioecy in Amborella trichopoda: evidence for genetically based sex determination and its consequences for inferences of the breeding system in early angiosperms. *Annals of botany* **119**: 591–597.

Binder BM. **2020**. Ethylene signaling in plants. *Journal of Biological Chemistry* **295**: 7710–7725.

Borin M. **2024**. Overcoming challenges in Cannabis sativa breeding research with conventional and biotechnological tools THESIS.

Boualem A, Troadec C, Camps C, Lemhemdi A, Morin H, Sari MA, Fraenkel-Zagouri R, Kovalski I, Dogimont C, Perl-Treves R, *et al.* 2015. A cucurbit androecy gene reveals how unisexual flowers develop and dioecy emerges. *Science* **350**: 688–691.

Brewer C, Harrower M, Sheesley B, Woodruff A, Heyman D. **2002**. ColorBrewer 2.0.

Bürstenbinder K, Rzewuski G, Wirtz M, Hell R, Sauter M. **2007**. The role of methionine recycling for ethylene synthesis in Arabidopsis. *Plant Journal* **49**: 238–249.

Carey SB, Aközbek L, Lovell JT, Jenkins J, Healey AL, Shu S, Grabowski P, Yocca A, Stewart A, Jones T, *et al.* 2024a. ZW sex chromosome structure in Amborella trichopoda. *Nature Plants* **10**.

Carey SB, Bentz PC, Lovell JT, Akozbek LM, Havill JS, Padgitt-Cobb L, Lynch RC, Allsing N, Osmanski A, Easterling KA, *et al.* 2024b. The evolution of heteromorphic sex chromosomes in plants. *bioRxiv*: 1–28.

Chen X, Schulz-Trieglaff O, Shaw R, Barnes B, Schlesinger F, Källberg M, Cox AJ, Kruglyak S, Saunders CT. **2016a**. Manta: rapid detection of structural variants and indels for germline and cancer sequencing applications. *Bioinformatics (Oxford, England)* **32**: 1220–1222.

Chen H, Sun J, Li S, Cui Q, Zhang H, Xin F, Wang H, Lin T, Gao D, Wang S, *et al.* 2016b. An ACC Oxidase Gene Essential for Cucumber Carpel Development. *Molecular Plant* **9**: 1315–1327.

Chen Y, Xu Y, Luo W, Li W, Chen N, Zhang D, Chong K. **2013**. The F-box protein OsFBK12 targets OsSAMS1 for degradation and affects pleiotropic phenotypes, including leaf senescence, in rice. *Plant Physiology* **163**: 1673–1685.

Chen H, Zhao Z, Chen J, Mertens J, Van de Poel B, Li D, Chen K. **2025**. The Yang cycle in plants: a journey of methionine recycling with fascinating metabolites and enzymes. *Plant Hormones* **1**: 0–0.

Chen Y, Zou T, McCormick S. **2016c**. S-adenosylmethionine synthetase 3 is important for pollen tube growth. *Plant Physiology* **172**: 244–253.

Cossard GG, Pannell JR. **2021**. Enhanced leaky sex expression in response to pollen limitation in the dioecious plant Mercurialis annua. *Journal of Evolutionary Biology* **34**: 416–422.

Danecek P, Auton A, Abecasis G, Albers CA, Banks E, DePristo MA, Handsaker RE, Lunter G, Marth GT, Sherry ST, *et al.* 2011. The variant call format and VCFtools. *Bioinformatics* **27**: 2156–2158.

DiMatteo J, Kurtz L, Lubell-Brand JD. **2020**. Pollen appearance and in vitro germination varies for five strains of female hemp masculinized using silver thiosulfate. *HortScience* **55**: 547–549.

Dowling CA, Shi J, Toth JA, Quade MA, Smart LB, McCabe PF, Schilling S, Melzer R. **2024**. A FLOWERING LOCUS T ortholog is associated with photoperiod-insensitive flowering in hemp (Cannabis sativa L.). *Plant Journal*: 1–21.

Eilbeck K, Lewis SE, Mungall CJ, Yandell M, Stein L, Durbin R, Ashburner M. **2005**. The Sequence Ontology: a tool for the unification of genome annotations. *Genome biology* **6**: 1–12.

Emms DM, Kelly S. **2015**. OrthoFinder: solving fundamental biases in whole genome comparisons dramatically improves orthogroup inference accuracy. *Genome Biology* **16**: 1–14.

Fattel L, Lawrence-Dill CJ. **2025**. GO Big or Go Home: A New Gene Ontology Subset that Improves Plant Gene Function Prediction. *bioRxiv*: 1–23.

Ferfuia C, Zuliani F, Danuso F, Piani B, Cattivello C, Dorigo G, Baldini M. **2021**. Performance and stability of different monoecious hemp cultivars in a multi-environments trial in north-eastern Italy. *Agronomy* **11**: 1–15.

Flajšman M, Slapnik M, Murovec J. **2021**. Production of Feminized Seeds of High CBD Cannabis sativa L. by Manipulation of Sex Expression and Its Application to Breeding. *Frontiers*

in Plant Science **12**: 1–12.

Galoch E. **1978**. The hormonal control of sex differentiation in dioecious plants of hemp (Cannabis sativa). *Acta Societatis Botanicorum Poloniae* **47**: 153–162.

García A, Aguado E, Garrido D, Martínez C, Jamilena M. **2020**. Two androecious mutations reveal the crucial role of ethylene receptors in the initiation of female flower development in Cucurbita pepo. *Plant Journal* **103**: 1548–1560.

Gaudet P, Dessimoz C. **2017**. Gene Ontology: Pitfalls, Biases, and Remedies. In: Dessimoz C, Škunca N, eds. Methods in Molecular Biology. New York, NY: Springer New York, 189–205.

Giese MW, Lewis MA, Giese L, Smith KM. **2015**. Development and validation of a reliable and robust method for the analysis of cannabinoids and terpenes in cannabis. *Journal of AOAC International* **98**: 1503–1522.

Grassa CJ, Weiblen GD, Wenger JP, Dabney C, Poplawski SG, Timothy Motley S, Michael TP, Schwartz CJ. **2021**. A new Cannabis genome assembly associates elevated cannabidiol (CBD) with hemp introgressed into marijuana. *New Phytologist* **230**: 1665–1679.

Green G. **2005**. *The Cannabis Breeder's Bible- The definitive guide to marijuana genetics, cannabis botany and creating strains for the seed market*. San Francisco: Green Candy Press.

Ji G, Zhang J, Zhang H, Sun H, Gong G, Shi J, Tian S, Guo S, Ren Y, Shen H, *et al.* 2016. Mutation in the gene encoding 1-aminocyclopropane-1-carboxylate synthase 4 (CitACS4) led to andromonoecy in watermelon. *Journal of integrative plant biology* **58**: 762–765.

Jones M, Monthony AS. **2022**. Cannabis Propagation. In: Handbook of Cannabis Production in Controlled Environments. Boca Raton: CRC Press, 91–121.

Käfer J, Méndez M, Mousset S. **2022**. Labile sex expression in angiosperm species with sex chromosomes. *Philosophical Transactions of the Royal Society B: Biological Sciences* **377**.

Komai F, Masuda K. **2004**. Plasticity in sex expression of spinach (Spinacia oleracea) regenerated from root tissues. *Plant Cell, Tissue and Organ Culture* **78**: 285–287.

Kramer CY. **1956**. Extension of Multiple Range Tests to Group Means with Unequal Numbers of Replications. *Biometrics* **12**: 307.

Kurtz LE, Brand MH, Lubell-Brand JD. **2020**. Production of tetraploid and triploid hemp. *HortScience* **55**: 1703–1707.

Langfelder P, Horvath S. **2008**. WGCNA: an R package for weighted correlation network analysis. *BMC Bioinformatics* **9**: 559.

Lapierre É, Monthony AS, Torkamaneh D. **2023a**. Genomics-based taxonomy to clarify cannabis classification. *Genome*.

Lapierre É, de Ronne M, Boulanger R, Torkamaneh D. **2023b**. Comprehensive Phenotypic Characterization of Diverse Drug-Type Cannabis Varieties from the Canadian Legal Market. *Plants* **12**: 1–17.

Li H. **2013**. Aligning sequence reads, clone sequences and assembly contigs with BWA-MEM.

Li Q, Guo W, Chen B, Pan F, Yang H, Zhou J, Wang G, Li X. **2021**. Transcriptional and Hormonal Responses in Ethephon-Induced Promotion of Femaleness in Pumpkin. *Frontiers in Plant Science* **12**.

Lin H, Liao Z, Zhang L, Yu Q. **2016**. Transcriptome analysis of the male-to-hermaphrodite sex reversal induced by low temperature in papaya. *Tree Genetics and Genomes* **12**.

Love MI, Huber W, Anders S. **2014**. Moderated estimation of fold change and dispersion for RNA-seq data with DESeq2. *Genome Biology* **15**: 1–21.

Lubell JD, Brand MH. **2018**. Foliar sprays of silver thiosulfate produce male flowers on female hemp plants. *HortTechnology* **28**: 743–747.

McDonald JH. **2014**. *Handbook of Biological Statistics*. Baltimore: Sparky House Publishing.

McLaren W, Gil L, Hunt SE, Riat HS, Ritchie GRS, Thormann A, Flicek P, Cunningham F. **2016**. The Ensembl Variant Effect Predictor. *Genome Biology* **17**: 1–14.

Monthony AS, Bagheri S, Zheng Y, Jones AMP. **2021a**. Flower power: floral reversion as a viable alternative to nodal micropropagation in Cannabis sativa. *In Vitro Cellular & Developmental Biology - Plant* **21**: 1–13.

Monthony AS, Kyne ST, Grainger CM, Jones AMP. **2021b**. Recalcitrance of Cannabis sativa to de novo regeneration; a multi-genotype replication study (KR Davis, Ed.). *PLOS ONE* **16**: e0235525.

Monthony AS, Page SR, Hesami M, Jones AMP. **2021c**. The Past, Present and Future of *Cannabis sativa* Tissue Culture. *Plants* **10**: 185.

Monthony AS, de Ronne M, Torkamaneh D. **2024**. Exploring ethylene-related genes in Cannabis sativa: implications for sexual plasticity. *Plant Reproduction*.

Moon Y-H, Lee YJ, Koo SC, Hur M, Huh YC, Chang J-K, Park WT. **2020**. Effect of Timing of Ethephon Treatment on the Formation of Female Flowers and Seeds from Male Plant of Hemp (Cannabis sativa L.). *The Plant Resources Society of Korea* **33(6)**: 682–688.

Mudge EM, Brown PN, Murch SJ. **2019**. The Terroir of *Cannabis*: Terpene Metabolomics as a Tool to Understand *Cannabis sativa* Selections. *Planta Medica* **85**: 781–796.

NCBI. **2023**. Cannabis sativa 'Pink Pepper' genome assembly GCA_029168945.1/ASM2916894v1.

Nei M, Li WH. **1979**. Mathematical model for studying genetic variation in terms of restriction endonucleases. *Proceedings of the National Academy of Sciences* **76**: 5269–5273.

Okonechnikov K, Conesa A, García-Alcalde F. **2015**. Qualimap 2: advanced multi-sample quality control for high-throughput sequencing data.

Orozco LR, Weaver AE, Pauli CC, Grassa CJ, Vergara D, Baptista A, White K, Emery BF, Castro NRM, Guerrero RF, *et al.* 2025. Unraveling Cross-Cellular Communication in Cannabis sativa Sex Determination: A Network Ontology Transcript Annotation (Nota) Analysis.

Otto SP, Pannell JR, Peichel CL, Ashman TL, Charlesworth D, Chippindale AK, Delph LF,

Guerrero RF, Scarpino S V., McAllister BF. **2011**. About PAR: The distinct evolutionary dynamics of the pseudoautosomal region. *Trends in Genetics* **27**: 358–367.

Page SRG, Monthony AS, Jones AMP. **2021**. DKW basal salts improve micropropagation and callogenesis compared with MS basal salts in multiple commercial cultivars of Cannabis sativa. *Botany* **99**: 269–279.

Piepho HP. **2004**. An algorithm for a letter-based representation of all-pairwise comparisons. *Journal of Computational and Graphical Statistics* **13**: 456–466.

van de Poel B, Bulens I, Markoula A, Hertog MLATM, Dreesen R, Wirtz M, Vandoninck S, Oppermann Y, Keulemans J, Hell R, *et al.* 2012. Targeted systems biology profiling of tomato fruit reveals coordination of the Yang cycle and a distinct regulation of ethylene biosynthesis during postclimacteric ripening. *Plant Physiology* **160**: 1498–1514.

Van de Poel B, Vandenzavel N, Smet C, Nicolay T, Bulens I, Mellidou I, Vandoninck S, Hertog MLATM, Derua R, Spaepen S, *et al.* 2014. Tissue specific analysis reveals a differential organization and regulation of both ethylene biosynthesis and E8 during climacteric ripening of tomato. *BMC Plant Biology* **14**.

Pommerrenig B, Feussner K, Zierer W, Rabinovych V, Klebl F, Feussner I, Sauera N. **2011**. Phloem-Specific expression of Yang cycle genes and identification of novel Yang cycle enzymes in Plantago and Arabidopsis. *Plant Cell* **23**: 1904–1919.

Prentout D, Razumova O, Rhoné B, Badouin H, Henri H, Feng C, Käfer J, Karlov G, Marais GAB. **2020**. An efficient RNA-seq-based segregation analysis identifies the sex chromosomes of Cannabis sativa. *Genome Research* **30**: 164–172.

Punja ZK, Holmes JE. **2020**. Hermaphroditism in Marijuana (Cannabis sativa L.) Inflorescences – Impact on Floral Morphology, Seed Formation, Progeny Sex Ratios, and Genetic Variation. *Frontiers in Plant Science* **11**: 1–20.

Quinlan AR, Hall IM. **2010**. BEDTools: a flexible suite of utilities for comparing genomic features. *Bioinformatics* **26**: 841–842.

Rajagopalan PA, Saraf-Levy T, Lizhe A, Perlp-Treves R. **2004**. Increased femaleness in transgenic cucumbers that over-express an ethylene receptor. In: Lebeda A, Paris HS, eds. Progress in cucurbit genetics and breeding research. Proceedings of Cucurbitaceae 2004, the 8th EUCARPIA meeting on Cucurbit Gentics and Breeding. Olomouc, 525–531.

Ram HYM, Jaiswal VS. **1972**. Induction of male flowers on female plants of Cannabis sativa by gibberellins and its inhibition by abscisic acid. *Planta* **105**: 263–266.

Rau A, Gallopin M, Celeux G, Jaffrézic F. **2013**. Data-based filtering for replicated high-throughput transcriptome sequencing experiments. *Bioinformatics* **29**: 2146–2152.

Reed J. **1914**. Morphology of *Cannabis sativa* L.

Resnick JS, Wen C-KCK, Shockey JA, Chang C. **2006**. REVERSION-TO-ETHYLENE SENSITIVITY1, a conserved gene that regulates ethylene receptor function in Arabidopsis. *Proceedings of the National Academy of Sciences* **103**: 7917–7922.

Roy J, Monthony AS, Torkamaneh D. **2025**. DESeq2-MultiBatch: Batch Correction for Multi-Factorial RNA-seq Experiments. *bioRxiv*.

Rzewuski G, Cornell KA, Rooney L, Bürstenbinder K, Wirtz M, Hell R, Sauter M. **2007**. OsMTN encodes a 5′-methylthioadenosine nucleosidase that is up-regulated during submergence-induced ethylene synthesis in rice (Oryza sativa L.). *Journal of Experimental Botany* **58**: 1505–1514.

Sather DN, Jovanovic M, Golenberg EM. **2010**. Functional analysis of B and C class floral organ genes in spinach demonstrates their role in sexual dimorphism. *BMC Plant Biology* **10**.

Shi J, Schilling S, Melzer R. **2024a**. Morphological and genetic analysis of inflorescence and flower development in hemp (Cannabis sativa L .). *bioRxiv*.

Shi J, Toscani M, Dowling CA, Schilling S, Melzer R. **2024b**. Identification of genes associated with sex expression and sex determination in hemp (Cannabis sativa L.). *bioRxiv*.

Solano R, Stepanova A, Chao Q, Ecker JR. **1998**. Nuclear events in ethylene signaling: A transcriptional cascade mediated by ETHYLENE-INSENSITIVE3 and ETHYLENE-RESPONSE-FACTOR1. *Genes and Development* **12**: 3703–3714.

Spitzer-Rimon B, Duchin S, Bernstein N, Kamenetsky R. **2019**. Architecture and florogenesis in female *Cannabis sativa* plants. *Frontiers in Plant Science* **10**: 1–11.

Stephens M. **2017**. False discovery rates: A new deal. *Biostatistics* **18**: 275–294.

Thomas TD. **2004**. In vitro modification of sex expression in mulberry (Morus alba) by ethrel and silver nitrate. *Plant Cell, Tissue and Organ Culture* **77**: 277–281.

Tian J, Zhang F, Zhang G, Li X, Wen C, Li H. **2024**. A long noncoding RNA functions in pumpkin fruit development through S -adenosyl- L -methionine synthetase. *Plant Physiology* **195**: 940–957.

Torkamaneh D, Laroche J, Tardivel A, O'Donoughue L, Cober E, Rajcan I, Belzile F. **2018**. Comprehensive description of genomewide nucleotide and structural variation in short-season soya bean. *Plant Biotechnology Journal* **16**: 749–759.

Toth JA. **2022**. Elucidating the genetic control of qualitative traits in hemp.

Toth JA, Stack GM, Cala AR, Carlson CH, Wilk RL, Crawford JL, Viands DR, Philippe G, Smart CD, Rose JKC, *et al.* 2020. Development and validation of genetic markers for sex and cannabinoid chemotype in Cannabis sativa L. *GCB Bioenergy* **12**: 213–222.

Tsuji H. **2017**. Molecular function of florigen. *Breeding Science* **67**: 327–332.

Uygun S, Peng C, Lehti-Shiu MD, Last RL, Shiu SH. **2016**. Utility and Limitations of Using Gene Expression Data to Identify Functional Associations. *PLoS Computational Biology* **12**: 1–27.

Waduwara-Jayabahu I, Oppermann Y, Wirtz M, Hull ZT, Schoor S, Plotnikov AN, Hell R, Sauter M, Moffatt BA. **2012**. Recycling of methylthioadenosine is essential for normal vascular development and reproduction in Arabidopsis. *Plant Physiology* **158**: 1728–1744.

Wang Q, Zeng X, Song Q, Sun Y, Feng Y, Lai Y. **2020**. Identification of key genes and modules in response to Cadmium stress in different rice varieties and stem nodes by weighted gene co-expression network analysis. *Scientific Reports* **10**: 9525.

Waters Corporation. **2019**. *Waters Kairos Amino Acid Kit*. Milford.

Welling MT, Deseo MA, Bacic A, Doblin MS. **2021**. Untargeted Metabolomic Analyses Reveal Chemical Complexity of Dioecious Cannabis Flowers. *Australian Journal of Chemistry* **74**: 463–479.

Wickham H. **2009**. *ggplot2: Elegant Graphics for Data Analysis*. New York, NY: Springer New York.

Zhang J, Shi J, Ji G, Zhang H, Gong G, Guo S, Ren Y, Fan J, Tian S, Xu Y. **2017**. Modulation of Sex Expression in Four Forms of Watermelon by Gibberellin, Ethephone and Silver Nitrate. *Horticultural Plant Journal* **3**: 91–100.

Zheng Y. **2022**. *Handbook of Cannabis Production in Controlled Environments* (Y Zheng, Ed.). Boca Raton: CRC Press.

Supplementary Table Captions

Supplementary Table 1 Cutting, vegetative and flowering growth conditions. Following rooting of cuttings, all plants were grown in controlled growth chambers. Male flowers (MF); female flowers (FF); induced female flowers (IFF); induced male flowers (IMF); as needed (PRN), Photosynthetic Photon Flux Density (PPFD).

Supplementary Table 2 Primer sequences used for sexing in a PACE assay, table extracted from Toth (2022).

Supplementary Table 3 Cannabinoid standards used in the cannabinoid quantification by UPLC-PDA. All standards were purchased from Agilent.

Supplementary Table 4 ACC and SAM standard concentrations. WS: Working solution.

Supplementary Table 5 ACC and SAM Calibration Range Before/After Derivatization with AccQ-Tag.

Supplementary Table 6 UPLC Gradient Elution Program Adapted from Kairos et al. (2019). The table outlines the gradient conditions used for chromatographic separation of ACC and SAM. Mobile phase A consists of 0.1% formic acid in water, while mobile phase B consists of 0.1% formic acid in acetonitrile.

Supplementary Table 7 Optimized Xevo TQ-S Mass Spectrometry Parameters for ACC and SAM Analysis.

Supplementary Table 8 Multiple Reaction Monitoring (MRM) Transitions for ACC and SAM Detection. m/z: refers to the mass-to-charge ratio of the ions detected; sd: denotes single dissociation, indicating that the precursor ion undergoes a single-step fragmentation before detection.

Supplementary Table 9 TargetLynx V4.1 Processing Parameters for ACC and SAM Quantification.

Supplementary Table 10 Metadata and RNA-seq quality control metrics for samples included in this study. Columns include sample name, genotype, genetic sex, tissue type, sample timepoint, treatment (Ctrl = control; ET = ethephon; STS = Silver thiosulfate), RNA integrity number (RIN) following sample RNA extraction, sequencing depth (coverage, ×), GC content (%), and average mapping quality following alignment with STAR and post-alignment QC using Qualimap. The final two columns indicate whether each sample passed internal quality filters and was retained for downstream weighted gene co-expression network analysis (WGCNA) and differential expression analysis (DESeq2), respectively.

Supplementary Table 11 Results of the F-test from the ANOVA for the percentage of *C. sativa* florets which underwent sex change.

Supplementary Table 12 Cannabinoid content (% w/w) of mature female flowers for the genotypes used in the present study and the analytical limit of quantification (LOQ) and limit of detection (LOD) for the cannbinoids analyzed. ND indicates that the sample was below the limit of detection. The cannabinoid abbreviations are as follows: tetrahydrocannabinolic acid (THCA), delta-9-tetrahydrocannabinol (Δ9-THC), cannabidiolic acid (CBDA), cannabidiol (CBD), cannabigerolic acid (CBGA), cannabigerol (CBG), cannabichromene (CBC), cannabinol (CBN), tetrahydrocannabivarin (THCV), and cannabidivarin (CBDV).

Supplementary Table 13 *C. sativa* ERGs as identified through homology analysis using the current reference genome ('Pink Pepper'; NCBI, 2023), X and Y haplotypes from the Otto II genotype, and the previous reference genome, Cs10 (Grassa *et al.*, 2021). Chr: chromosome number.

Supplementary Table 14 Genetic diversity analysis of XX and XY genotypes Deadly Kernel, La Rosca and Panama Pupil V4.

Supplementary Table 15 Quantification data (ug/g fresh weight) of 1-aminocyclopropane-1-carboxylic acid (ACC) and detection of S-adenosylmethionine (SAM) by UPLC-MS.

Supplementary Table 16 ERGs identified within treatment-associated modules from the XX and XY network before differential gene expression filtering. Module-trait correlations (r) indicate the relationship between each module and treatment (STS for XX and ethephon for XY) or time points (Day 1 and Day 14). Intramodular connectivity (kME) reflects the centrality of each gene within its assigned module.

Supplementary Figures Captions

Supplemental Figure 1 Representative timeline of floral development in MF, IMF, FF and IFF of *C. sativa* 'Deadly Kernel' (DK) and 'Panama Pupil V4' (PP) from 7 to 28 days after the photoperiod shift from long day to short day. N/A indicates photo not available for a given time/treatment.

1267

Supplemental Figure 2 Genomic distribution and predicted impact of SNPs and structural variants (SVs) in the 47 ERGs of the six C. sativa samples. A) Schematic representation of a gene structure and its surrounding regulatory regions (5 kb upstream and downstream), highlighting genomic elements considered in the analysis. Regions are color-coded based on their predicted impact, ranging from modifier (low impact, mostly regulatory) to low, moderate, or high impact (potential functional consequences protein function). Distribution of SNPs (B) and SVs (C) categorized by their predicted impact and localization. D) Distribution of modifier impact variants (SNPs and SVs) across the 47 ERGs. E) Distribution of low to high impact variants identified in the 47 ERGs.

1268

1269

Supplemental Figure 3 Endogenous ACC concentrations and their correlation with CsCTR1-LIKE expression in C. sativa leaves during floral transition. A) ACC quantification at vegetative (day 0) and flowering (day 1) stages across experimental groups. Error bars represent standard error of the estimated marginal means. Different letters indicate significant differences among groups (Tukey's HSD, $\alpha = 0.05$). B) Spearman correlation heatmap depicting the relationship between CsCTR1-LIKE (LOC115706236) expression and ACC concentration across treatment groups. A significant negative correlation ($\rho = -0.8$, $p \leq 0.001$) is observed in XX Day 0 – FF. Statistical significance for Spearman correlations was categorized as follows: $p \leq 0.001$, ***; $p \leq 0.01$, **; $p \leq 0.05$, *; correlations with $p > 0.05$ were considered non-significant.

1270

Supplemental Figure 4 WGCNA module identification and correlation analysis. A, B) Clustering dendrogram for XX (A) and XY (B) plants. C-D) Module-trait correlation heatmaps of identified modules correlated with treatment and day. Modules significantly associated with the traits with identified with $|cor| > 0.5$ and p value ≤ 0.05, and are indicated by asterisks as follows: $p \leq 0.001$, ***; $p \leq 0.01$, **; $p \leq 0.05$, *; correlations with $p > 0.05$ were considered non-significant. Red and blue color notes positive and negative correlation between a given module and trait pair.

1271

Supplemental Figure 5 Differential expression data contrasting control (MF or FF) and sex changed (IFF or IMF) plants at day 1 and 14 using the 24 ERGs identified from WGCNA. Genes which show genotype-independent behaviour (gray highlight) were retained for further analysis.